ACS Chemical Neuroscience

Article

ITH14001, a CGP37157-nimodipine hybrid designed to regulate calcium homeostasis and oxidative stress, exerts neuroprotection in cerebral ischemia

Izaskun Buendia, Giammarco Tenti, Patrycja Michalska, Iago Méndez-López, Enrique Luengo, Michele Satriani, Juan Fernando Padin Nogueira, Manuela G. López, María Teresa Ramos, Antonio G García, J. Carlos Menéndez, and Rafael León

ACS Chem. Neurosci., **Just Accepted Manuscript** • DOI: 10.1021/acschemneuro.6b00181 • Publication Date (Web): 12 Oct 2016

ITH14001, a CGP37157-nimodipine hybrid designed to regulate calcium homeostasis and oxidative stress, exerts neuroprotection in cerebral ischemia

Izaskun Buendia, [#,‡] *Giammarco Tenti,* [†,‡] *Patrycja Michalska,* [#,§] *Iago Méndez-López,* [#,§] *Enrique Luengo,* [#,§] *Michele Satriani,* [#,†] *Fernando Padín-Nogueira,* [#,§] *Manuela G. López,* [#,§] *Mª. Teresa Ramos,* [†] *Antonio G. García,* [#,§] *J. Carlos Menéndez**[†] *and Rafael León**[#,§]

Instituto Teófilo Hernando y Departamento de Farmacología y Terapéutica, Facultad de Medicina. Universidad Autónoma de Madrid, 28029 Madrid, Spain.

† Departamento de Química Orgánica y Farmacéutica, Facultad de Farmacia, Universidad Complutense, 28040 Madrid, Spain.

§ Instituto de Investigación Sanitaria, Servicio de Farmacología Clínica, Hospital Universitario de la Princesa, 28006 Madrid, Spain.

RECEIVED DATE (to be automatically inserted after your manuscript is accepted if required according to the journal that you are submitting your paper to)

ABSTRACT: During brain ischemia, oxygen and glucose deprivation induces calcium overload, extensive oxidative stress, neuroinflammation and, finally, massive neuronal loss. In the search of a neuroprotective compound to mitigate this neuronal loss, we have designed and synthesized a new multitarget hybrid (ITH14001) directed at the reduction of calcium overload by acting on two regulators of calcium homeostasis; the mitochondrial Na^+/Ca^{2+} exchanger (mNCX) and L-type voltage dependent calcium channels (VDCCs). This compound is a hybrid of CGP37157 (mNCX inhibitor) and nimodipine (L-type VDCCs blocker), and its pharmacological evaluation revealed a moderate ability to selectively inhibit both targets. These activities conferred concentration-dependent neuroprotection in two models of Ca^{2+} overload, such as toxicity induced by high K^+ in the SH-SY5Y cell line (60 % protection at 30 μM) and veratridine in hippocampal slices (26 % protection at 10 μM). It also showed neuroprotective effect against oxidative stress, an activity related to its nitrogen radical scavenger effect and moderate induction of the Nrf2-ARE pathway. Its Nrf2 induction capability was confirmed by the increase of the expression of the antioxidant and anti-inflammatory enzyme heme-oxygenase I (3-fold increase). In addition, the multitarget profile of ITH14001 led to anti-inflammatory properties, shown by the reduction of nitrites production induced by lipopolysaccharide in glial cultures. Finally, it showed protective effect in two acute models of cerebral ischemia in hippocampal slices, excitotoxicity induced by glutamate (31 % protection at 10 μM) and oxygen and glucose deprivation (76 % protection at 10 μM), reducing oxidative stress and iNOS deleterious induction. In conclusion, our hybrid derivative showed improved neuroprotective properties when compared to its parent compounds CGP37157 and nimodipine.

KEYWORDS. Calcium dyshomeostasis, cerebral ischemia, multitarget drugs, mitochondrial NCX, voltage dependent calcium channels, Nrf2 inducers.

INTRODUCTION

Calcium ion (Ca^{2+}) is the most important second messenger implicated in neurotransmission as well as other cellular processes, such as the production of reactive

oxygen or nitrogen species (ROS, RNS),[1] mitochondrial bioenergetics,[2] neurogenesis,[3] autophagy[4] and cell life/death signalling.[5] The pleiotropic activity of this ion makes necessary a tight control of its concentration fluctuations in all cellular compartments and thus cells have developed a plethora of systems to strongly control the amplitude and the temporal extension of its signals.[6] However, these Ca^{2+} buffering systems fail under certain pathological conditions leading to dysregulation of Ca^{2+} homeostasis.[7] Futile Ca^{2+} cycling affects many cellular processes, principally the life/death equilibrium leading to apoptosis and cell death. Neurodegenerative diseases are a prominent example where Ca^{2+} dyshomeostasis has been related to disease onset and development.[8] In fact, neuronal death induced by Ca^{2+} dysregulation has been widely reported in several neurological disorders such as Alzheimer´s disease,[9] Parkinson´s disease[10] or cerebral ischemia.[11] Among these, cerebrovascular accidents are the second leading cause of death and the first cause of disability in the world.[12]

Ischemia, commonly known as stroke, occurs after the interruption of the cerebral blood flow, causing a decreased delivery of oxygen and nutrients into the brain.[13] Oxygen and glucose deprivation (OGD) during ischemia leads to cytosolic calcium ($[Ca^{2+}]_c$) overload prompted by a massive release of the excitatory amino acid glutamate.[14] Thereafter, mitochondrial failure induces the production of free radical species that is exacerbated during the reoxygenation (reox) phase. At the same time, the elevated levels of oxidative stress and the initial neuronal death induce glial activation and neuroinflammation. Reactive glia increases the production of free radicals and releases pro-inflammatory cytokines,[15] contributing to a massive neuronal death.[16]

Currently, the only approved treatment for ischemic stroke is the tissue plasminogen activator (tPA), a drug that accelerates thrombus removal, although its use is highly restricted due to its small therapeutic window. In search for alternative approaches,

neuroprotection represents a useful instrument to prevent the onset and to combat the progression of this pathological condition. In this context, the most widely accepted targets to develop neuroprotective agents against ischemic stroke are: the reduction of $[Ca^{2+}]_c$ overload, the decrease of ROS production during the reox phase and the reduction of glial activation. However, clinical trials of single-target drugs aimed at one of these pathological processes have failed so far, probably because the complexity of the pathological cascade of events involved in the pathogenesis of cerebral ischemia. It has thus become apparent during the last years that multitarget drugs should be potentially more effective for the treatment of this condition.[17]

In order to reduce the initial $[Ca^{2+}]_c$ overload, several targets have been proposed, including the mitochondrial Na^+/Ca^{2+} exchanger (mNCX) and the voltage dependent calcium channels (VDCCs). The mNCX protein has been widely used as a neuroprotective target as it regulates mitochondrial Ca^{2+} cycling (mCC).[18] It is considered responsible for about 50% of the $[Ca^{2+}]_c$ overload occurring during ischemia, due to increased levels of intracellular Na^+.[19] Along with a reduction of $[Ca^{2+}]_c$ overload, the mNCX blockade strategy induces mitochondrial calcium ($[Ca^{2+}]_m$) elevation increasing the activity of Ca^{2+} dependent dehydrogenases and augmenting ATP synthesis and thus favouring neuronal viability. The mNCX antagonist that has received most attention is 7-chloro-5-(2-chlorophenyl)-1,5-dihydro-4,1-benzothiazepin-2(3*H*)-one (CGP37157, figure 1) which acts as a neuroprotective drug against ischemia.[18, 20] Furthermore, this compound reduced neuronal damage in *in vivo* models of cerebral ischemia.[21]

On the other hand, VDCC and specifically the L-type VDCCs are considered the most permeable channels to Ca^{2+} and the most important contributors to $[Ca^{2+}]_c$ overload in pathological conditions.[22] Focusing on ischemic stroke, nimodipine reduces infarct size

after stroke and improves the clinical outcome in acute ischemic stroke in animal models.[23] However, clinical trials have recurrently failed to show efficacy,[24] which has been related to the hypotension caused by the potent blockade of vascular smooth muscle cells[25] associated to the high selectivity of 1,4-dihydropyridines as blockers of the cardiovascular L-type VDCCs ($Ca_V1.2$) relative to the neuronal subtype ($Ca_V1.3$).[26] The relevance of the L-type VDCCs as a therapeutic target has been reinforced by the recent finding of an important link between Ca^{2+} entry through L-type VDCCs and the production of free radical species.[27] Thus, L-subtype VDCCs blockade simultaneously reduces Ca^{2+} overload and oxidative stress, two of the main pathological features in ischemic stroke.[26]

Regarding oxidative damage, the phase II antioxidant and anti-inflammatory response is a highly promising target against oxidative stress and neuroinflammation occurring in ischemic stroke. Several inducers of the nuclear factor E2-related factor 2 (Nrf2) transcriptional factor, the master regulator of phase II antioxidant response, have demonstrated high neuroprotection in different animal models.[28] Furthermore, 3-butylphthalide (NBP), a component of celery oil that acts as an Nrf2 inducer, has found clinical use in China to treat ischemic stroke.[29]

Taking into account these precedents, we have recently proposed the multitarget combination of mNCX antagonism and L-type VDCC blockade, as an interesting strategy to re-establish the mCC reducing $[Ca^{2+}]_c$ overload, and antioxidant effect as complementary mechanisms of action to provide neuronal survival.[30]

Under these premises, we report here the design, synthesis, and pharmacological evaluation of a new CGP37157-nimodipine hybrid, named ITH14001, endowed with VDCC blocker and mNCX antagonist properties. Furthermore, calcium influx through L-type VDCCs induces the production of free radicals and thus a moderate blockade of

this channel is expected to mitigate oxidative stress occurring during the reoxygenation phase in ischemia. The study of this compound as a calcium cycle regulator and neuroprotective agent in several models of $[Ca^{2+}]_c$ overload, oxidative stress, cerebral ischemia and neuroinflammation is reported.

RESULTS AND DISCUSSION

Rational design of a multitarget neuronal calcium stabilizer. Against the aforementioned background, we undertook a rational pharmacophore-directed design towards a multitarget calcium stabilizer. Our initial concept involved linking two structurally active fragments, namely the benzothiazepine derivative CGP37157 to interact with mNCX, and a 1,4-dihydropyridine derivative to target the L-type VDCCs, in order to intervene directly in the modulation of both the cellular and mCC. As the CGP-37157 structure did not offer many options to establish a link with another molecule without affecting its activity, we selected as the mNCX-blocking partner a benzodiazepinone analogue of the compound. This choice emerged from previous structure-activity-relationships of mNCX inhibitors, which showed that simple replacement of the sulphur atom at the 4-position by a nitrogen atom bearing a 2-hydroxyethyl substituent afforded a compound with a comparable activity to the parent CGP37157.[31] We envisaged that this dimethylene chain could act as the linker between the benzodiazepine moiety and the dihydropyridine group, whereas the OH could be used for the formation of an ester with one of the carbonyl functions located at C-3 or C-5 of the dihydropyridine. On the other hand, we decided to use nimodipine as the dihydropyridine component of our hybrid due to its well-known behaviour as a calcium channel blocker, and also because one of its ester groups has a good structural similarity with the planned linker (figure 1).

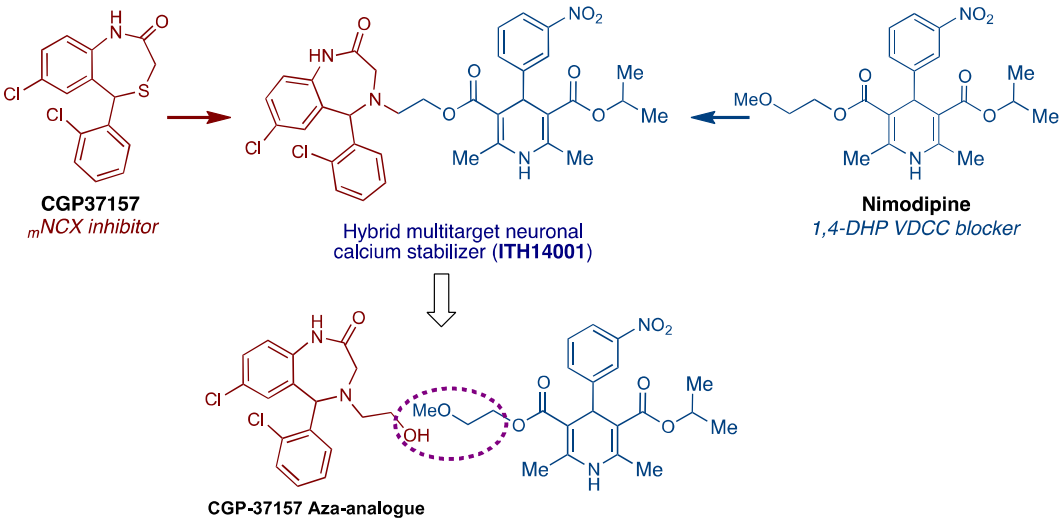

Figure 1. Rational design of the multitarget neuronal calcium stabilizer ITH14001.

Chemistry. We started by synthesizing initially the aza-analogue of CGP37157 *via* a modification of the literature method.[31] As illustrated in Scheme 1, 2-amino-2',5-dichlorobenzophenone **2** was condensed with 2-aminoethanol to afford the imine **3** that was subsequently reduced to the β-aminoalcohol **4**. With this compound in hand, we proceeded to the formation of the diazepine ring by its treatment with bromoacetyl bromide in a one-pot, multi step fashion, obtaining compound **5** as the result of the reaction of the β-hydroxy group with a second equivalent of bromoacetyl bromide. After subsequent hydrolysis of **5** by classical base-promoted saponification we obtained the expected aza-analogue of CGP37157 **6** in an overall 47% yield.

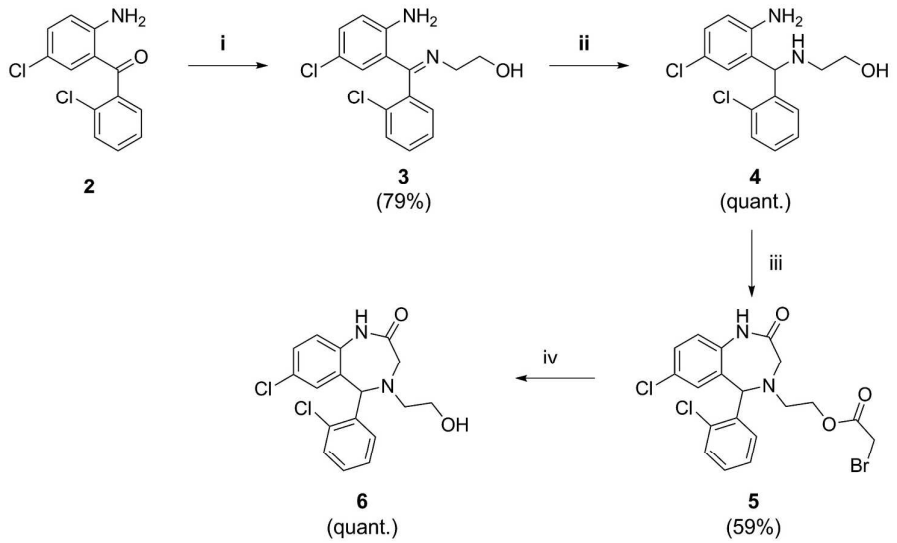

Scheme 1. Synthesis of the aza-analogue of CGP37157 **6**. **Reagents and conditions**: (i) 2-aminoethanol (neat), 140 ºC, 20 h; (ii) $NaBH_3(CN)$, MeOH/AcOH, 0 ºC to room temperature, 18 h; (iii) (a) bromoacetyl bromide, 0 ºC to room temperature, 17 h; (b) DIEA, 50 ºC, 5 h; (iv) 2 M aqueous KOH, MeOH, room temperature, 2 h.

Based on our previous experience on the synthesis of bioactive dihydropyridine derivatives[26] we decided to synthesize the target compound in a multicomponent fashion, employing a modified three-component Hantzsch dihydropyridine synthesis to build the nimodipine fragment. Thus, we prepared on one hand, the β-ketoester **7** employing a transesterification of methyl acetoacetate with compound **6** in the presence of the acidic ion exchange resin Amberlyst® 15[32] and, on the other hand, the conjugated enone **8** by using the classical conditions for the Knoevenagel condensation.[33] The final three-component reaction between compounds **7**, **8** and ammonium acetate in refluxing ethanol afforded the desired hybrid ITH14001 in good yield (72%) (Scheme 2).

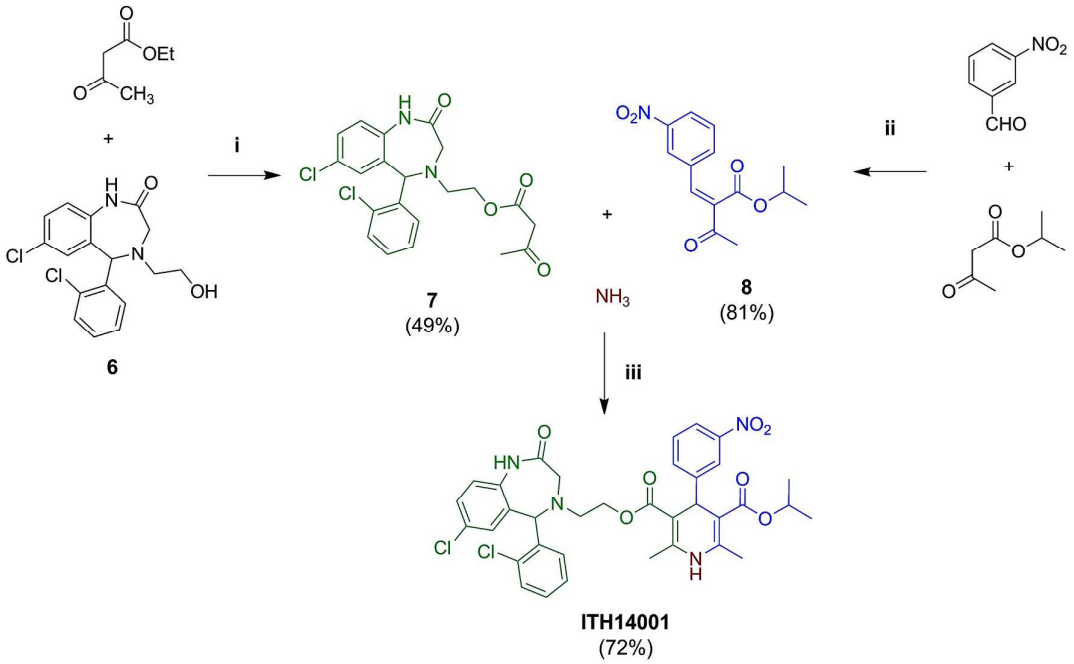

Scheme 2. Multicomponent synthesis of the hybrid compound ITH14001. **Reagents and conditions**: (i) Amberlist-15, toluene, reflux, 15 h; (ii) Piperidine, AcOH, benzene, reflux, 16 h; (iii) EtOH, reflux, 15 h.

Pharmacology.

Compound ITH14001 modulates both the L-type VDCCs and the mNCX transporter. In order to determine the potential activity of our compound over the mCC and L-type VDCCs we used primary cultures of bovine chromaffin cells (BCCs), a well-accepted model of paraneuron where we established the percentage of VDCCs-subtypes expressed by these cells.[34] As shown in figure 2, ITH14001 did not change the $[Ca^{2+}]_c$ peak in BCCs (figure 2A). Nevertheless, it altered the kinetics of $[Ca^{2+}]_c$ clearance at 10 μM, augmenting the time constant (τ) of the slow component of the $[Ca^{2+}]_c$ clearance from 32.9 ± 2.8 s to 52.6 ± 5.1 s ($p < 0.005$) (figure 2B). This result shows that although ITH14001 does not block the Ca^{2+} entry through VDCCs in BCCs, it mitigates the clearance of $[Ca^{2+}]_c$ by mitochondria, suggesting that it might block the mNCX.[35] Furthermore, ITH14001 does not alter the VDCCs currents in BCCs as shown

in figure 2C; this correlates with the observation that the compound did not alter the peak $[Ca^{2+}]_c$ transient generated by K^+ in fura-2-loaded BCCs (figure 2A).

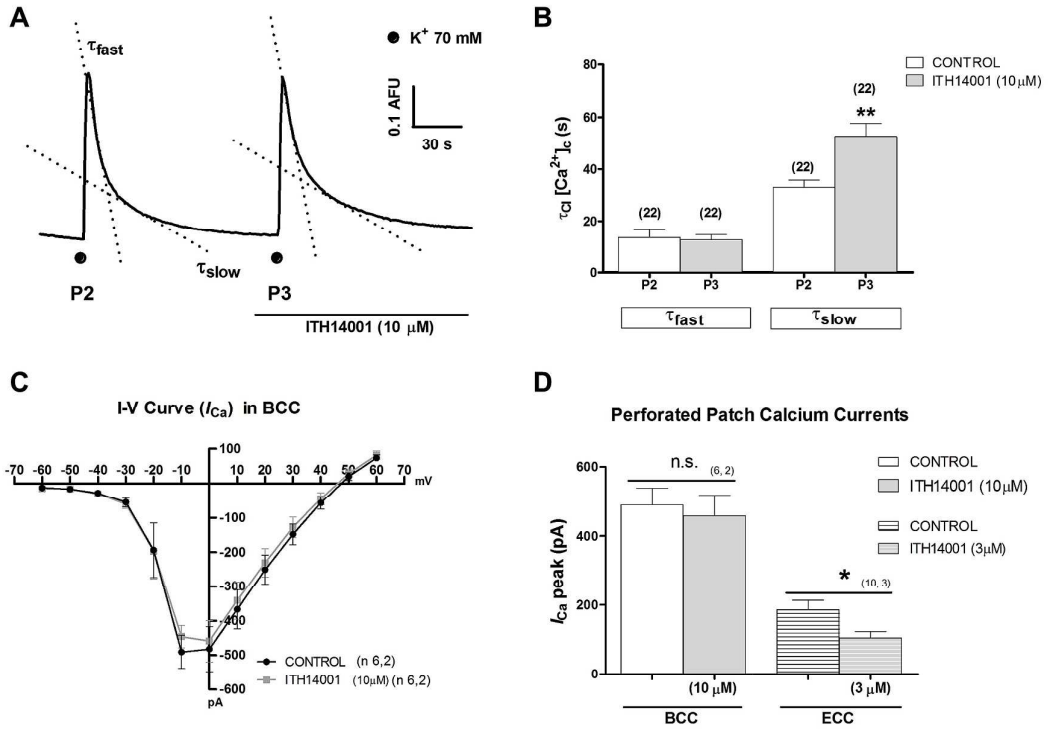

Figure 2. A) Representative traces of $[Ca^{2+}]_c$ evoked by K^+ pulses (5 s, 70 mM) in BCCs. $[Ca^{2+}]_c$ measurements were done with Fura-2 AM dye (1 h incubation, 10 μM). P2 and P3 represent the second and the third pulse under compound (ITH14001, 10 μM) incubation. B) Quantification of both (fast and slow) clearance time constant of the $[Ca^{2+}]_c$ peaks represented in A. C) Intensity-voltage (I-V) calcium current curve elicited by 50-ms depolarizing pulses in BCCs under the perforated patch configuration. I-V curves were performed perfusing the cells with tyrode medium (Control) or tyrode with ITH14001 (10 μM). D) Quantification of the calcium current peak (I_{Ca}) in BCCs or in embryo chromaffin cells (ECCs) without (control) or with ITH14001 treatment in BCCs (3 μM) and in ECCs (10 μM). Data are mean ± SEM of triplicates of four independent experiments: *$p < 0.05$ compared with control; **$p < 0.01$, compared with control conditions.

To further analyze whether the effect of ITH14001 is specific over mNCX, the voltage-dependent calcium currents in chromaffin cells from rat embryo (ECC) were measured. The rat ECCs is an excellent model to study the L-type VDCC due to its high expression in this type of cells.[34b] In ECCs current through L-type channel corresponds to 60 % of the total,[36] differently from BCCs where it only accounts for 20 %. In this case, the electrophysiological experiments showed a significant blockade of the peak I_{Ca} (186.1 ± 27.6 pA) in the control *vs.* under ITH14001 pre-incubation (105.0 ± 6.0 pA, figure 2D) ($p < 0.05$). Therefore, we can conclude that ITH14001 modulates calcium signalling by blocking specifically the mNCX and also the L-type VDCC. Given its relatively low potency to target L-type VDCCs, it is expected that compound ITH14001 would have less hypotensive effects compared classical dihydropyridines which are known to have a potent vasodilatory effect.

As described, the ischemic cascade starts with the mitochondrial failure and $[Ca^{2+}]_c$ overload followed by intensive oxidative stress damage and glial activation during the reoxygenation phase. The dual mechanism of action of ITH14001 reduces the initial $[Ca^{2+}]_c$ overload acting over the mNCX and L-type VDCCs. This target combination helps to mitigate futile mCC and $[Ca^{2+}]_c$ overload favouring mitochondria stabilization and energy recovery. The moderate activity over L-type VDCCs might also be of interest since it can reduce secondary effects over the cardiovascular system, an effect related to the failure of nimodipine in clinical trials for cerebral ischemia.[26]

ITH14001 exerts neuroprotective effects against the toxicity elicited by $[Ca^{2+}]_c$ overload. We next evaluated the potential neuroprotective effect of compound ITH14001 in two different cytotoxic models related to $[Ca^{2+}]_c$ overload; a) high $[K^+]$ and b) veratridine. First we used the SH-SY5Y neuroblastoma cell line exposed to a depolarizing concentration of K^+ during 24 h, which causes $[Ca^{2+}]_c$ overload and

mitochondrial dysfunction inducing a 45 % cell death.[26] Cells were co-incubated with increasing concentrations of ITH14001 or reference compounds (nimodipine and CGP37157) and high K^+ (70 mM) during 24 h. Thereafter, cell viability was assayed by the MTT method.[37] Our hybrid compound exerted neuroprotection at 10 μM (25 % protection) and 30 μM (60 % protection) ($p < 0.001$). Compared to reference compounds, nimodipine and CGP37157, with neuroprotective effects of 47 and 40 %, respectively, ITH14001 showed a higher neuroprotective effect at 30 μM (figure 3), although the differences were not significant.

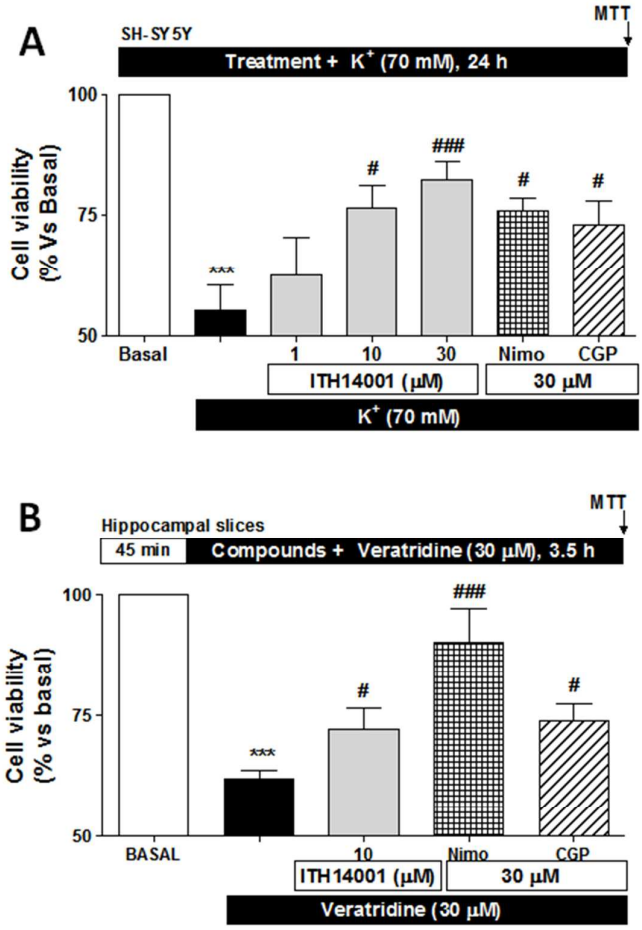

Figure 3. Neuroprotective effect of ITH14001 against $[Ca^{2+}]_c$ overload: A) neuroprotective effect of ITH14001 against the cytotoxic effect induced by high K^+ (70 mM). Cells were co-incubated with increasing concentrations of ITH14001 or control compounds (nimodipine and CGP37157, 30 μM) and high K^+ during 24 h. B)

Cytoprotective effect against the toxicity elicited in rat hippocampal slices by veratridine (30 μM) during 3.5 h alone or co-incubated with the indicated treatments. Data are expressed as mean ± SEM of four different experiments in triplicate. ***p < 0.001 compared with basal conditions; $^{###}p < 0.001$ and $^{\#}p < 0.05$ compared with the corresponding toxic stimulus.

The study of the neuroprotective profile of hybrid ITH14001 against $[Ca^{2+}]_c$ overload was completed using veratridine as toxic stimulus, in rat hippocampal slices.[38] This alkaloid induces $[Na^+]_c/[Ca^{2+}]_c$ overload by blocking Na^+ channels inactivation, leading to mitochondria being unable to modulate Na^+ and Ca^{2+} and thus implicating the mNCX. Using a protocol previously described by our group, we employed 30 μM of veratridine during 3.5 h that induced 38 % of cell death (figure 3B).[18a] In this model, CGP37157 achieved maximum protection at 30 μM[18a] and thus we used CGP37157 and nimodipine at this concentration for comparative purposes. ITH14001 was used at 10 μM as it was able to protect almost at the same extent of that achieved with 30 μM in the previous model. As shown in figure 3B, our hybrid derivative was able to induce a 26 % of neuroprotection, a value very close of that achieved by CGP37157 (31 %) at 30 μM with no significant differences. Nimodipine showed a very potent neuroprotective effect being able to rescue 76 % of viability at 30 μM.

Compound ITH14001 exerts antioxidant properties. Among the different alterations observed in brain ischemia, oxidative stress and neuroinflammation are two key elements that trigger neuronal death. The uncontrolled entry of Ca^{2+} through the L-type VDCCs has been recently related directly to an increase of ROS,[10] and thus the moderate blockade of L-type VDCCs by hybrid derivative ITH14001 might improve its neuroprotective effect against oxidative stress. Therefore, we used the rotenone and oligomycin A combination (rote/olig) in the SH-SY5Y neuroblastoma cell line as

oxidative stress model to test this hypothesis. The toxic combination increases ROS production, damaging mitochondria, reducing ATP production and causing cell death simulating the pathological events occurring in cerebral ischemia.[39] As shown in figure 4A, rote/olig caused 38 % of cell death, which was prevented by ITH14001 in a concentration dependent manner from 0.3 μM to 30 μM. In this case, melatonin and nimodipine were included as positive control and reference compound. CGP37157 was not included since it is toxic at the concentration of 30 μM in SH-SY5Y neuroblastoma cells (see supporting information) and it was unable to protect in this oxidative stress model.[18b, 40] Compared to positive control melatonin, ITH14001 showed similar protection at 0.3 and 1 μM, and higher neuroprotective effect was achieved at 10 μM ($p < 0.05$) and 30 μM ($p < 0.01$). Compared to nimodipine, hybrid derivative ITH14001 showed an improved neuroprotective effect (figure 4A).

In view of the protective effect against oxidative stress we envisaged the possibility of an additional scavenger effect in our hybrid. We first used the oxygen radical absorbance capacity (ORAC) assay to test the ROS scavenging effect, but our compound was inactive in this assay (data not shown). We then submitted the compound to the α,α-diphenyl-β-picrylhydrazyl (DPPH) assay, in which the radicals generated are RNS. Interestingly, ITH14001 showed a good activity in this assay, being two times more potent than melatonin at the same concentration as a RNS scavenger ($p < 0.05$) (figure 4B).

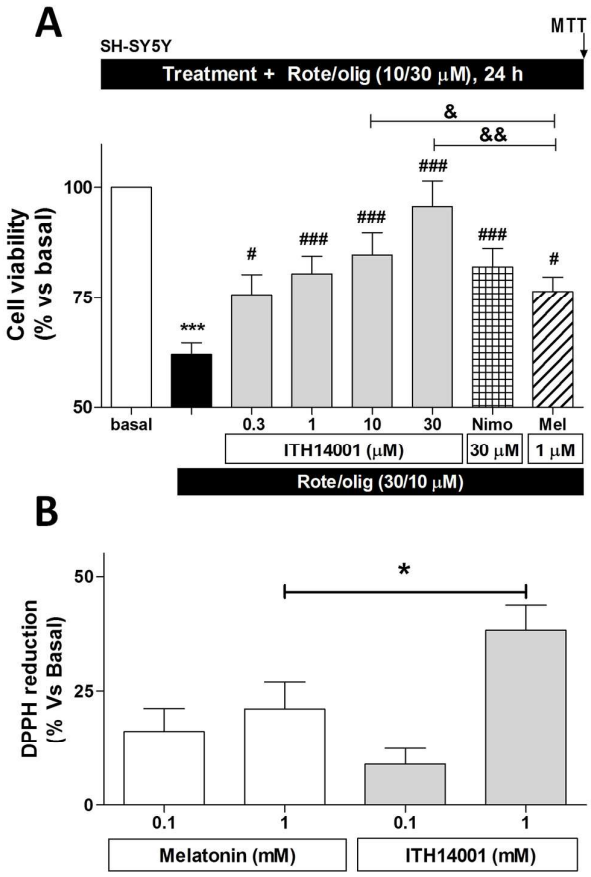

Figure 4. Neuroprotective effect against oxidative stress and DPPH reduction effect of ITH14001: A) protective effect of increasing concentrations of ITH14001 against the toxicity induced by rotenone/oligomycin A (30/10 μM) with a co-incubation protocol during 24 h. Data are expressed as means ± SEM of five different experiments in triplicate. ***$p < 0.001$ compared to basal conditions; $^{###}p < 0.001$ and $^{\#}p < 0.05$ compared to toxic stimulus. $^{\&\&}p < 0.01$ and $^{\&}p < 0.05$ compared to melatonin. . B) Scavenger effect of ITH14001 in the DPPH assay compared to the antioxidant neurohormone melatonin. Values are expressed as percentage of DPPH radical reduction as mean ± SEM of four different experiments in triplicate. *$p < 0.05$ compared with melatonin 1 mM.

ITH14001 reduces the toxicity elicited by glutamate and oxygen and glucose deprivation in brain hippocampal slices. As summarized above, glutamate-induced excitotoxicity is an important process causing neuronal death through $[Ca^{2+}]_c$ overload[41]

and mitochondrial failure in cerebral ischemia.[42] In fact, one of the most widely used *in vitro* models of stroke is the glutamate-induced toxicity in rat hippocampal slices.[40] As we have demonstrated, ITH14001 exhibits Ca^{2+} regulatory activity and antioxidant properties and thus we considered of interest to explore its potential protective effect in this neurotoxicity model. The experimental protocol used is described in the upper part of figure 5A; after the stabilization period (45 min, 34 ºC), rat hippocampal slices were incubated with glutamate alone (1 mM), or co-incubated with increasing concentrations of ITH14001 (1, 10 and 30 μM) or control compounds, nimodipine (30 μM) and CGP37157 (30 μM), during 4 h at 37 ºC. Under these conditions glutamate induced 25 % reduction of cell-viability (measured by MTT reduction) (figure 5A), a value similar to that previously reported.[43] Interestingly, ITH14001 reduced this neuronal lesion at all concentrations assayed, achieving a 25%, 76% and 60% neuroprotection at 1, 10 and 30 μM, respectively. The parent compounds nimodipine (68 % protection) and CGP37157 (67 % protection), used at 30 μM exhibited an effect similar to that achieved by ITH14001 at 3-fold lower concentration (10 μM, 76 % protection).

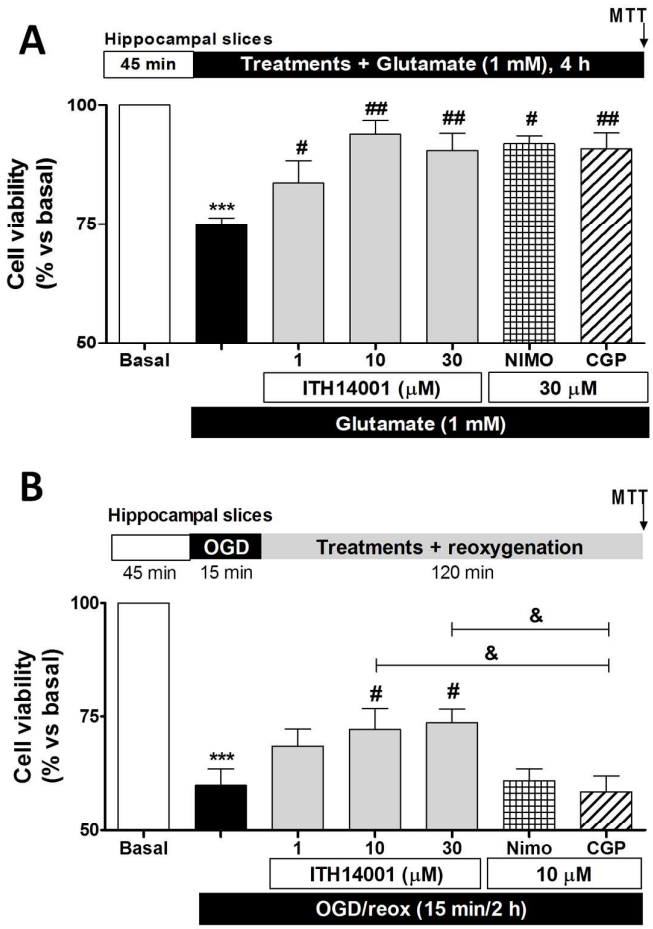

Figure 5. ITH14001 protected rat hippocampal slices against the excitotoxicity elicited by glutamate and the toxicity induced by OGD/reox. A) After the stabilization period (45 min), slices were incubated with glutamate (1 mM) alone or co-incubated with the compounds during 4 h. Thereafter, viability was determined by the MTT method. B) After 45 min stabilization slices were subjected to OGD (15 min) followed by reoxygenation (2 h). Treatments were incubated after the OGD period, during the reoxygenation phase. Thereafter, viability was determined by the MTT method. Data are expressed as mean ± SEM of five different experiments in triplicate. $^{***}p < 0.001$ compared with basal conditions; $^{\#\#}p < 0.01$ and $^{\#}p < 0.05$ compared with the correspondent toxic stimulus. $^{\&}p < 0.05$ compared with CGP37157.

The pharmacological profile and neuroprotective properties of the ITH14001 prompted us to use a more physiological brain ischemia model. We selected the oxygen

and glucose deprivation (OGD) followed by reoxygenation (reox) model in rat hippocampal slices. In this model, the OGD period (15 min) induces mitochondrial depolarization, glutamate release and $[Ca^{2+}]_c$ overload. During the reoxygenation phase, there is a massive release of ROS and RNS.[44] We have selected a post-OGD incubation protocol to better reproduce the clinical condition where patients are treated after the brain ischemic episode has occurred. Rat hippocampal slices subjected to 15 min of OGD followed by 2 h of reox caused 40 % cell death ($p < 0.001$), whereas the post-OGD treatment with increasing concentrations of ITH14001 afforded 31 % ($p < 0.05$) and 34 % ($p < 0.05$) neuroprotection at 10 and 30 μM, respectively. Interestingly, the neuroprotective effect exerted by ITH14001 was not observed for the parent compounds, CGP37157 and nimodipine, at the concentration of 10 μM, showing a statistically significant ($p < 0.05$) better neuroprotection than both at this concentration. The neuroprotection values for both parent compounds are in line with results previously described in our group.[26, 40]

ITH14001 reduces ROS production and iNOS over-expression induced in the OGD/reox ischemia model. As previously described, increased ROS production and neuroinflammation are two of the best-described alterations occurring after brain ischemic episode.[45] OGD/reox causes an increase of 95 % of ROS production in hippocampal slices, measured as H_2DCFDA increase of fluorescence (figure 6A and 6C). In slices treated with ITH14001 (10 μM), ROS levels were significantly reduced almost to basal levels ($p< 0.001$). This reduction might be related to its ability to modulate Ca^{2+} currents (figure 1), reducing Ca^{2+} overload, which stabilize the mitochondria. Additionally, the partial blockade of L-type VDCC (figure 1) might help to reduce oxidative stress. Furthermore, our compound can trap RNS thereby reducing nitrosative damage (figure 4B).[46]

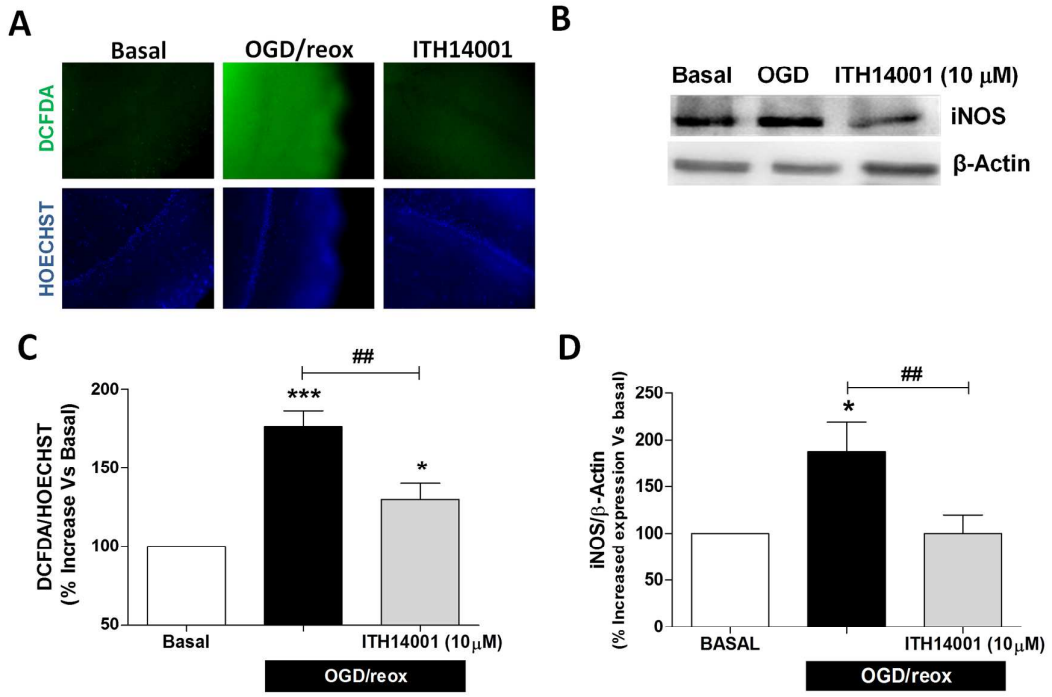

Figure 6. ITH14001 reduces ROS production and iNOS expression in rat hippocampal slices after OGD/reox. ROS production measured as H_2DCFDA fluorescence intensity increase after OGD-reox period. Slices were subjected to the same OGD/reox protocol loaded with the fluorescent dye during the stabilization period. Compound ITH14001 was incubated at 10 μM after the 15 min OGD period, during the reox phase. A) Representative microphotographs of ROS production and C) ROS production quantification. Western-blot analysis of iNOS expression in hippocampal slices subjected to OGD/reox alone or incubated post-OGD with ITH14001 (10 μM). B) Representative western blot traces and D) iNOS expression quantification. Data are expressed as mean ± SEM of five different experiments in quadruplicate. ***$p < 0.001$ compared with basal conditions; $^{\#\#}p < 0.005$ and $^{\#}p < 0.05$ compared with the corresponding toxic stimulus.

In an effort to study the neuroinflammatory component of the OGD/reox model in hippocampal slices, we measured the induction of inducible nitric oxide synthase (iNOS) enzyme occurring during the OGD/reox. As shown in figure 6B and 6D, OGD/reox doubled the expression of iNOS in rat hippocampal slices ($p < 0.05$). Post-

OGD treatment with ITH14001 (10 μM) completely prevented the deleterious over-expression of this pro-inflammatory enzyme ($p < 0.005$). Thus, ITH14001 was able to reduce neuroinflammation occurring during ischemia, a complementary activity to its Ca^{2+} regulation and antioxidant properties. In the aggregate, these properties are an interesting multitarget combination to prevent brain ischemia damage.

ITH14001 is able to induce the phase II antioxidant and anti-inflammatory response in primary glial cultures. Together with the Ca^{2+} cycling regulation and the antioxidant activity, we were interested in further demonstrating the potential anti-inflammatory activity of compound ITH14001 as part of its mechanism of action. ITH14001 was able to reduce OGD/reox damage by reducing ROS production (figure 5B and 6A) and iNOS expression (figure 6B), the latter result indicating a potential direct effect over the activation of glial cells. In this line, the protection afforded by our compound against oxidative stress might be related not only to its calcium regulation and antioxidant activities, but also to an increase in the antioxidant capability of the cell. The Nrf2 factor is the master regulator of the phase II antioxidant and anti-inflammatory response, and small compounds can induce its activity to trigger a neuroprotective response against oxidative stress.[28] Among others, Nrf2 induces the expression of the antioxidant and anti-inflammatory enzyme heme-oxygenase-1 (HO-1) and the catalytic subunit (GCLc) of glutathione-C-ligase, the enzyme that catalyses the limiting step of the *de novo* synthesis of glutathione. On the other hand, it has been recently demonstrated that nimodipine is able to protect against oxidative stress by moderately inducing the Nrf2 response.[47] Thus, we tested the possibility of Nrf2 induction by ITH14001 compared with CGP37157 and nimodipine at the same concentration (30 μM) (Nrf2 induction dose-response curves of all compounds are included in the Supporting Information). Figure 7A shows that compound ITH14001 was able to

significantly ($p < 0.001$) increase luciferase expression by 2.1 fold. This Nrf2-induction ability was significantly ($p < 0.05$) higher than that observed for nimodipine (1.9 fold induction). In this model, GGP37157 was completely unable to induce the Nrf2-ARE response at this concentration, being significantly less potent than our hybrid derivative ($p < 0.001$) (figure 7A).

ROS and RNS over-production are related to the increase in inflammatory cytokines observed after brain ischemia.[48] After demonstrating the antioxidant effect and Nrf2 induction capability of hybrid ITH14001, we were interested in elucidating its potential anti-inflammatory properties. For this purpose, primary glial cell cultures were exposed during 18 h to 1 μg/ml of lipopolysaccharide (LPS), which is widely used to cause an inflammatory response. Under these experimental conditions, the production of nitrites increased four times compared to basal conditions (figure 7B) ($p < 0.005$). Treatment with 1 and 10 μM of ITH14001 did not offer any anti-inflammatory effect; however, at 30 μM, it reduced nitrites production induced by LPS (figure 7B) by 71 % ($p < 0.05$). This anti-inflammatory activity complements the multitarget profile of our hybrid derivative, making it particularly attractive against brain ischemia.

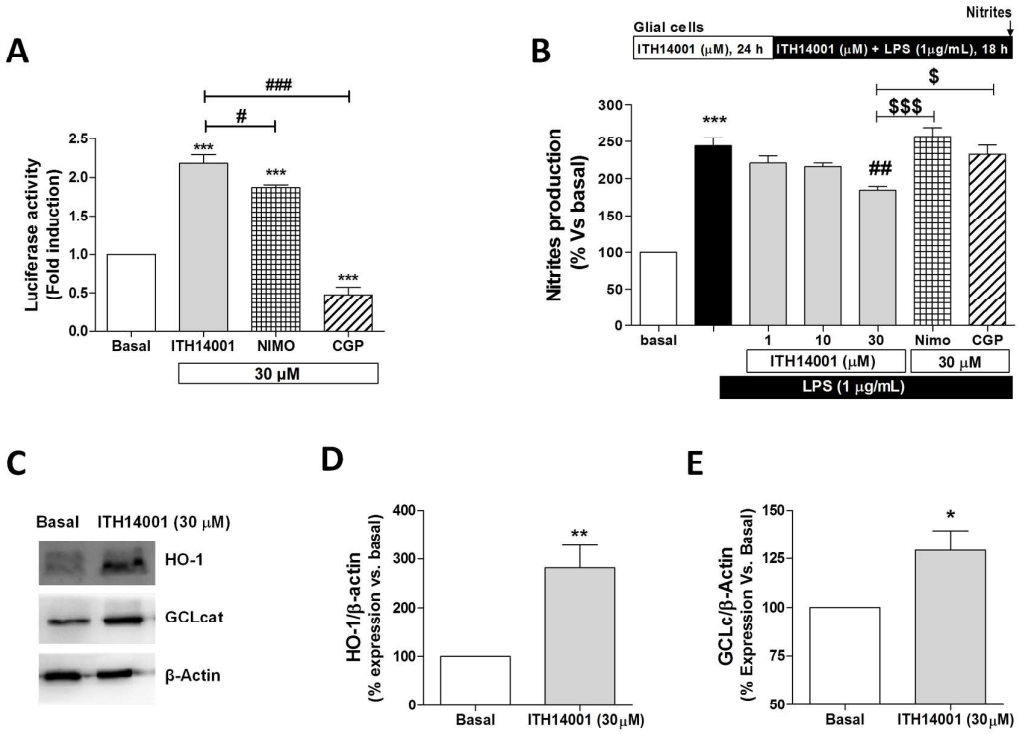

Figure 7. ITH14001 induces the expression of Nrf2-ARE pathway dependent enzymes in AREc32 and glial cells. A) Nrf2 induction in AREc32 cells by ITH14001, nimodipine and CGP37157 at 30 μM. Luciferase relative activity was normalized to control conditions assigning the value of 1. Data are expressed as mean ± SEM of duplicates of five different experiments. ***$p < 0.001$ compared to basal conditions; $^{###}p < 0.001$ and $^{\#}p < 0.05$ compared to ITH14001. B) Reduction of nitrite production by compound ITH14001 upon stimulation of primary glial cultures with LPS (1 μg/mL). Data were normalized to basal conditions (100 %). Data are expressed as mean ± SEM of five different experiments in triplicate. **$p < 0.005$ compared with basal conditions; $^{\#}p < 0.05$ compared with LPS-induced nitrite production. C) Western-blot analysis of HO-1 and GCLc enzymes induced by ITH14001 (30 μM) in glial cells primary cultures. D) Quantification of HO-1 and E) GCLc over-expression normalized to basal conditions induced by ITH14001 (30 μM). Data are expressed as mean ± SEM of four different cultures. **$p < 0.01$ and *$p < 0.05$ compared with basal conditions.

Additionally, we investigated the Nrf2-induction properties in glial cells as a potential mechanism of action to reduce oxidative stress and neuroinflammation. Thus, we measured the expression of HO-1 and GCLc in primary glial cultures, which would be involved in the antioxidant and anti-inflammatory effects of ITH14001. Mixed glial cells primary cultures were pre-treated with ITH14001 (30 μM) during 24 h. After this period, glial cells were processed to measure protein expression by western-blot (figure 7C). ITH14001 induced by 3-fold HO-1 enzyme ($p < 0.01$) (figure 7D) and by 40 % GCLc ($p < 0.05$) (figure 7E), compared to non-treated cells. Therefore, the extra antioxidant and anti-inflammatory effects observed with ITH14001 can be related, at least in part, to the induction of Nrf2 and the increased expression HO-1 and GCLc enzymes.

Finally, the new compound has shown no hepatotoxicity or neurotoxicity up to 30 μM (figure 8C and 7D) revealing a better safety profile compared to CGP37157, which was significantly toxic at 30 μM (figure 8A).

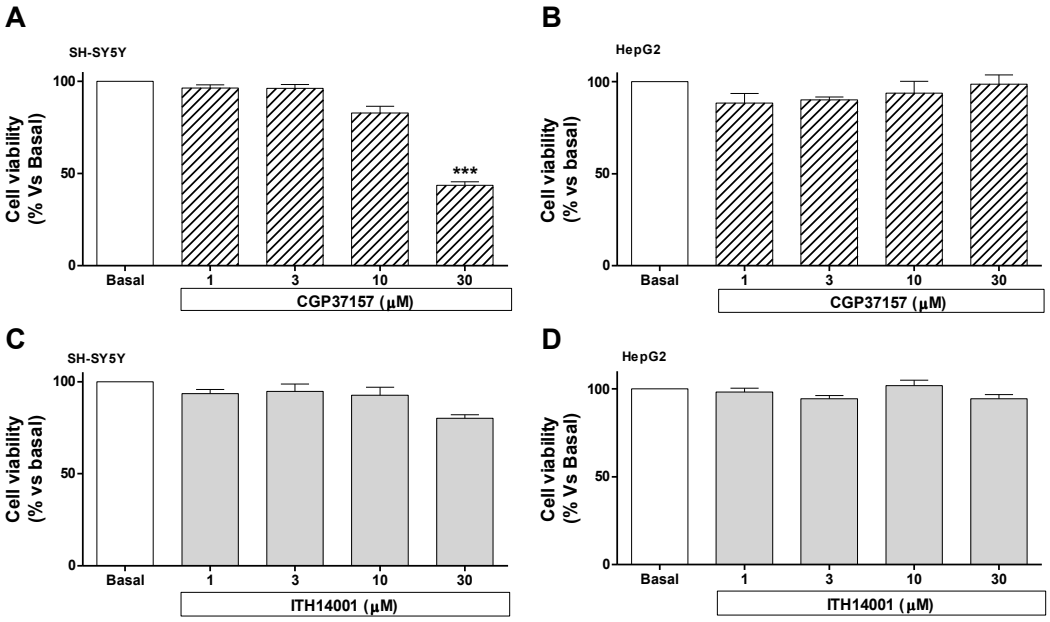

Figure 8: Cytotoxicity elicited by compound ITH14001 and CGP37157 in the neuroblastoma cell line SH-SY5Y and hepatotoxicity in the hepatocarcinoma HepG2

cells. Viability was measured as MTT reduction in presence of increasing concentrations of compounds. Data are expressed as mean ± SEM of four different experiments in triplicate. ***$p < 0.001$ compared to basal conditions.

CONCLUSIONS

In conclusion, compound ITH14001, designed as a hybrid of CGP37157 and nimodipine, caused neuroprotection on *in vitro* cellular and tissue slices models related to cerebral ischemia. In this report we demonstrate its activity over mNCX (figure 1) and VDCC being a moderate blocker. Both activities are related to the neuroprotection exerted by compound ITH14001 against $[Ca^{2+}]_c$ overload, being of interest in the first phase of ischemic damage. We also describe its antioxidant properties including RNS scavenger and Nrf2 induction capability that might be related to its neuroprotective activity against oxidative stress. Finally, we have also demonstrated its anti-inflammatory profile in primary glial cultures, which represent and improvement compared to its parent compounds. The plethora of activities demonstrated by hybrid ITH14001 are of high interest for the treatment of cerebral ischemia since this pathological condition exhibit a complex combination of pathological pathways related to Ca^{2+} dyshomeostasis, oxidative stress and neuroinflammation. Taken together, ITH14001 is a multitarget compound of potential interest for the treatment of brain ischemia conditions.

METHODS

Chemistry. All reagents (Aldrich, Fluka, SDS, Probus) and solvents (SDS), were of commercial quality and were used as received. Reactions were monitored by thin layer chromatography, on aluminium plates coated with silica gel with fluorescent indicator (SDS CCM221254). Separations by flash chromatography were performed on silica gel

(SDS 60 ACC 40-63 μm) or neutral alumina (Merck S22). Melting points were measured on a Reichert 723 hot stage microscope, and are uncorrected. Infrared spectra were recorded on an Agilent Cary630 FTIR spectrometer with a diamond ATR accessory for solid and liquid samples, requiring no sample preparation. NMR spectra were obtained on a Bruker Avance 250 spectrometer operating at 250 MHz for ^{1}H and 63 MHz for ^{13}C (CAI de Resonancia Magnética Nuclear, Universidad Complutense). NMR chemical shifts marked as * show that the assignment can be interchanged between two or more magnetic nuclei with similar chemical shifts. Elemental analyses were determined by CAI de Microanalisis Elemental, Universidad Complutense, using a Leco 932 CHNS combustion microanalyzer. Experimental procedures and characterization data for new compounds follow. For full experimental procedures and characterization data, see the Supporting Information.

Synthesis of 2-(7-chloro-5-(2-chlorophenyl)-2-oxo-2,3,4,5-tetrahydro-1*H*-benzo[*e*][1,4]diazepin-4-yl)ethyl 2-bromoacetate (5). To a stirred solution of **4** (2.116 g, 6.8 mmol) in 35 mL of CH_2Cl_2 at 0 °C was added bromoacetyl bromide (1.48 mL, 17.0 mmol), and stirring was continued at 0 °C for 1 hour and then at room temperature for 16 h. Diethylamine (17.4 mL, 100.0 mmol) was added, and the mixture was stirred at 50 °C for 5 h. The mixture was cooled to room temperature and diluted with CH_2Cl_2; the CH_2Cl_2 solution was washed with water and dried over anhydrous magnesium sulphate. After filtration, the filtrate was concentrated to dryness, and the crude product was purified using silica gel column chromatography (hexane:AcOEt 100/0 to 60/40) to give **5** as a white solid (1.894 g, 59%). Mp: 148-149 °C. IR (neat) ν 2948, 1733, 1664, 1025 cm^{-1}. ^{1}H NMR (250 MHz, $CDCl_3$) δ (ppm) 2.84-3.00 (m, 1H, one H of CH_2-β), 3.00-3.15 (m, 1H, one H of CH_2-β), 3.47 (d, J = 15.5 Hz, 1H, one H of CH_2-3), 3.58 (d, J = 15.5 Hz, 1H, one H of CH_2-3), 3.85 (s, 2H, CH_2-2), 4.14-4.29 (m, 1H, one H of

CH_2-α), 4.33-4.49 (m, 1H, one H of CH_2-α), 5.31 (s, 1H, CH-5), 7.05 (d, *J* = 8.5 Hz, 1H, CH-9), 7.25 (dd, *J* = 8.3, 2.2 Hz, 1H, CH-8), 7.45-7.29 (m, 4H, CH-6, CH-4', CH-5' and CH-6'), 7.60 (dd, *J* = 7.3, 1.5 Hz, 1H, CH-3'), 9.12 (s, 1H, CONH). ^{13}C NMR (63 MHz, $CDCl_3$) δ (ppm) 172.39 (C-2=O), 167.45 (C-1"=O), 137.26 (C-1'*), 137.02 (C-5a*), 134.90 (C-9a), 132.78 (C-6'*), 131.14 (CHAr), 130.93 (C-7*), 130.68 (CHAr), 130.50 (CHAr), 129.93 (CHAr), 129.34 (CHAr), 127.52 (CHAr), 122.56 (CHAr), 65.45 (CH-5), 64.17 (CH_2-α), 53.23 (CH_2-β), 52.30 (CH_2-3), 26.18 (CH_2-2"). Anal. Calcd. (%) for $C_{19}H_{17}BrCl_2N_2O_3$: C: 48.33, H: 3.63, N: 5.93; found: C: 47.96, H: 3.48, N: 6.06.

Synthesis of 2-(7-chloro-5-(2-chlorophenyl)-2-oxo-2,3,4,5-tetrahydro-1*H*-benzo[*e*][1,4] diazepin-4-yl)ethyl 3-oxobutanoate (7). A mixture of methyl acetoacetate (0.332 g, 2.85 mmol), **6** (1.053 g, 3 mmol) and Amberlyst-15 (10% by weight of β-ketoester, 0.033 g) in toluene (10 mL) was heated to 110 °C in a flask provided with a distillation condenser (Dean-Stark) to remove MeOH. After completion of the reaction, monitored by TLC, the catalyst was filtered off and the filtrate was concentrated and purified using silica gel column chromatography (CH_2Cl_2:AcOEt from 100:0 to 75:25) to give **7** as a pale brown solid (0.640 g, 49%). Mp 68-69 °C. IR (neat) ν 2918, 1712, 1665, 1034 cm^{-1}. ^{1}H NMR (250 MHz, $CDCl_3$) δ (ppm) 2.27 (s, 3H, CH_3-4"), 2.80-2.96 (m, 1H, one H of CH_2-β), 2.97-3.11 (m, 1H, one H of CH_2-β), 3.36-3.67 (m, 4H, CH_2-3 and CH_2-2"), 4.12-4.28 (m, 1H, one H of CH_2-α), 4.28-4.42 (m, 1H, one H of CH_2-α), 5.29 (s, 1H, CH-5), 6.61 (d, *J* = 2.3 Hz, 1H, CH-6), 6.98 (d, *J* = 8.5 Hz, 1H, CH-8), 7.18-7.47 (m, 4H, CH-9, CH-4', CH-5' and CH-6'), 7.54 (dd, *J* = 7.2, 2.2 Hz, 1H, CH-3'), 8.38 (s, 1H, CONH). ^{13}C NMR (63 MHz, $CDCl_3$) δ (ppm) 200.88 (C-3"=O), 172.62 (C-2=O), 167.38 (C-1"=O), 137.35 (C-1'*), 136.93 (C-5a*), 134.86 (C-9a), 132.80 (C-2'*), 131.10 (CHAr), 130.86 (C-7*), 130.67 (CHAr), 130.50 (CHAr), 129.89 (CHAr), 129.29 (CHAr), 127.49 (CHAr), 122.55 (CHAr), 65.42 (CH-5), 63.33

(CH_2-α), 53.24 (CH_2-β), 52.34 (CH_2-3), 50.35 (CH_2-2”), 30.66 (CH_3-4”). Anal. calcd (%) for $C_{21}H_{20}Cl_2N_2O_4$: C: 57.94, H: 4.63, N: 6.44; found: C: 57.82, H: 4.78, N: 6.33.

Synthesis of 3-(2-(7-chloro-5-(2-chlorophenyl)-2-oxo-2,3,4,5-tetrahydro-1*H*-benzo[*e*][1,4]diazepin-4-yl)ethyl) 5-isopropyl 2,6-dimethyl-4-(3-nitrophenyl)-1,4-dihydropyridine-3,5-dicarboxylate 1 (ITH14001). A solution of **7** (192 mg, 0.44 mmol) and ammonium acetate (68 mg, 0.88 mmol) in ethanol (2 mL) was stirred for 30 min at room temperature; **8** (122 mg, 0.44 mmol) was then added and the mixture was heated under reflux and stirred for 15 hours. After this time, the mixture was diluted with CH_2Cl_2 (20 mL), washed with water followed by brine, and dried over anhydrous magnesium sulfate. Evaporation of the solvent under reduced pressure left a crude that was purified using silica gel column chromatography (dichlorometane:ethyl acetate from 100:0 to 90:10) to give ITH14001 as a light yellow solid (218 mg, 72%). Mp: 149-150°C. IR (neat) ν 1675, 1526, 1348, 1101 cm^{-1}. ^1H NMR (250 MHz, $CDCl_3$) 2 isomers δ (ppm) 1.06 (d, *J* = 6.2 Hz, 3H, OCH(CH_3)$_2$ one isomer), 1.07 (d, *J* = 6.2 Hz, 3H, OCH(CH_3)$_2$ one isomer), 1.22 (d, *J* = 6.0 Hz, 3H, OCH(CH_3)$_2$ one isomer), 1.24 (d, *J* = 5.8 Hz, 3H, OCH(CH_3)$_2$ one isomer), 2.32 (s, 6H, C-6CH_3 two isomers), 2.37 (s, 3H, C-2CH_3 one isomer) 2.38 (s, 3H, C-2CH_3 one isomer), 2.77-3.04 (m, 4H, CH_2-β, two isomers), 3.35-3.56 (m, 4H, CH_2-3’ two isomers), 4.06-4.14 (m, 2H, CH_2-α one isomer), 4.23-4.39 (m, 2H, CH_2-α one isomer), 4.89-5.00 (m, 2H, OC*H*(CH_3)$_2$ two isomers), 5.06 (s, 1H, CH-4 one isomer), 5.12 (s, 1H, CH-4 one isomer), 5.16 (s, 1H, CH-5’ one isomer), 5.28 (s, 1H, CH-5’ one isomer), 5.73 (bs, 2H, NH-1 two isomers), 6.43 (d, *J* = 2.0 Hz, 1H, NH-1’ one isomer), 6.62 (d, *J* = 2.1 Hz, 1H, NH-1’ one isomer), 6.94 (d, *J* = 5.5 Hz, 1H, Ar*H* one isomer), 6.98 (d, *J* = 5.5 Hz, 1H, Ar*H* one isomer), 7.16-7.39 (m, 11H, Ar*H* two isomers), 7.52-7.55 (m, 1H, Ar*H* one isomer), 7.64 (d, *J* = 7.5 Hz, 2H, Ar*H* two isomers), 7.92-7.97 (m, 2H, Ar*H* two isomers), 8.23-8.04 (m, 4H,

Ar*H* two isomers). ^{13}C NMR (63 MHz, $CDCl_3$) 2 isomers δ (ppm) 172.35 (C-2'=O one isomer), 171.83 (C-2'=O one isomer), 167.26 (C-5 *C*=O* one isomer), 167.22 (C-5 *C*=O* one isomer), 166.96 (C-3 *C*=O* one isomer), 166.91 (C-3 *C*=O* one isomer), 150.28 (C-6* one isomer), 150.22 (C-6* one isomer), 148.53 (C-2* one isomer), 148.47 (C-2* one isomer), 145.64 (CNO_2* one isomer), 145.45 (CNO_2* one isomer), 144.84 (CAr* one isomer), 144.78 (CAr* one isomer), 137.46 (C-1"* one isomer), 137.30 (C-1"* one isomer), 137.02 (C-5a* one isomer), 136.82 (C-5a* one isomer), 135.01 (CHAr one isomers), 134.95 (CHAr one isomer), 134.82 (C-9a* one isomer), 134.81 (C-9a* one isomer), 133.01 (C-2"'* one isomer), 132.75 (C-2"* one isomer), 131.05 (CHAr one isomer), 130.96 (C-7 one isomer), 130.77 (CHAr + C-7 one isomer), 130.64 (CHAr one isomer), 130.55 (CHAr one isomer), 130.50 (CHAr one isomer), 130.33 (CHAr one isomer), 129.75 (CHAr one isomer), 129.67 (CHAr one isomer), 129.22 (CHAr one isomer), 128.99 (CHAr one isomer), 128.94 (CHAr one isomer), 127.50 (CHAr one isomer), 127.30 (CHAr one isomer), 123.59 (CHAr one isomer), 123.53 (CHAr one isomer), 122.46 (CHAr two isomers), 121.76 (CHAr two isomers), 104.24 (C-5 two isomers), 103.47 (C-3 one isomer), 103.29 (C-3 one isomer), 67.84 (O**C**H$(CH_3)_2$ two isomers), 65.35 (CH-5' one isomer), 65.07 (CH-5' one isomer), 61.74 (CH_2-α one isomer), 61.15 (CH_2-α one isomer), 53.30 (CH_2-β one isomer), 52.68 (CH_2-β one isomer), 52.48 (CH_2-3' two isomers), 40.41 (CH-4 one isomer), 40.33 (CH-4 one isomer), 22.52 (C-6 *C*H_3 two isomers OCH(*C*$H_3)_2$ one isomer), 22.19 (C-2 *C*H_3 one isomer), 20.37 (OCH(*C*$H_3)_2$ one isomer), 20.21 (OCH(*C*$H_3)_2$ one isomer), 20.04 (OCH(*C*$H_3)_2$ two isomer). MS (TOF-pos) m/z calcd for $C_{35}H_{34}Cl_2N_4O_7$ $[M+H]^+$ 693.187, found 693.042. Anal. calcd (%) for $C_{35}H_{34}Cl_2N_4O_7$: C: 60.61, H: 4.94, N: 8.08; found: C: 60.23, H: 4.94, N: 8.10.

Pharmacology. DMEM/F12, rotenone, oligomycin A, LPS (lipopolysaccharide), NEDA (N-(1-Naphthyl)ethylenediamine dihydrochloride), DAPSONE (4,4´-diamino-di-phenylsulfone) were obtained from Sigma (Madrid, Spain). 2,7-Dichlorofluorescein diacetate (H_2DCFDA) was purchased from Molecular Probes (Invitrogen, Madrid, Spain). Penicillin, pyruvate, and 5 % heat-inactivated fetal bovine serum (FBS), DMEM-glutamax, were purchased from Invitrogen. Luciferase Assay System (E1500) was purchased from Promega (Madison, WI, USA).

Animals. P3-10 or 3-months (300 g) male Sprague-Dawley (SD) rats were housed under controlled temperature and lighting conditions. Food and water were provided *ad libitum*. All the efforts were made to minimize number of animals and animal suffering. All the performed procedures were carried out following the Guide for the Care and Use of Laboratory Animals, which were pre-approved by the ethics committees for the care and use of animals in research of the Universidad Autónoma de Madrid, Spain, and according to the European Guidelines for the use and care of animals for research in accordance with the European Union Directive of 22 September 2010 (2010/63/UE) and with the Spanish Royal Decree of 1 February 2013 (53/2013).

Culture of Bovine Chromaffin cells. Bovine chromaffin cells (BCCs) were isolated from calves adrenal glands, following standard methods.[49] Cells were suspended in culture medium (DMEM) supplemented with fetal calf serum (5 %), cytosine arabinoside (10 μM), fluorodeoxyuridine (10 μM), streptomycin (50 μg/ml) and penicillin (50 IU/ml). Cells were plated on 12-mm diameter glass coverslips at low density (1.0 x 10^5 cells/coverslip) for patch-clamp studies. To study the changes of $[Ca^{2+}]_c$, cells density was 5 x 10^5 cells/coverslip (25-mm diameter glass coverslips). Primary cells cultures were kept in an incubator at 37°C, water-saturated and in a 5 % CO_2-95 % air atmosphere. Experiments were carried out 24 h thereafter.

Culture of rat embryos chromaffin cells. Sprague Dawley rats were housed individually under controlled temperature and lighting conditions. Food and water was provided *ad libitum*. Chromaffin cells were obtained from 18-day-old rat embryos following a protocol described for mice[50] with some modifications. The pregnant rat was killed by decapitation, and the fetuses were extracted and decapitated immediately. Adrenal glands were removed from the embryos and submersed in 0.5 ml of papain (20 U/ml) enzymatic solution for tissue digestion (20 min). 5 ml of culture medium with fetal calf serum (5 %) to stop the enzymatic reaction was then added. Cells were extracted mechanically by successive passes through 1000 µl plastic micropipette. The solution was then centrifuged (4 min at 400 rpm), the supernatant was removed and 0.8 to 1.5 ml of DMEM were added depending on the final cell density desired. A 100-µl drop of cell-containing solution was plated on glass poly-D-lysine-coated coverslips on 24-well plates (for patch-clamp experiments) or on 6-well plates (for cytosolic Ca^{2+} experiments), DMEM (0.5 ml for 24-well plates and 2 ml for 6-well plates) supplemented with 4 % fetal bovine serum, penicillin (50 IU/ml), and streptomycin (50 µg/ml) was added to each well after 45 min in incubator. Primary cells cultures were kept in an incubator at 37°C, water-saturated and in a 5 % CO_2-95 % air atmosphere. Experiments were carried out 24 h thereafter.

Recording of calcium currents. Calcium currents (I_{Ca}) were recorded at room temperature by patch-clamp technique (using perforated-patch mode with amphotericin B as the permeating agent).[51] Tight seals (>5 GΩ) were achieved in a standard extracellular Tyrode solution for recording I_{Ca} composed of the following (in mM): 137 NaCl, 1 $MgCl_2$, 2 $CaCl_2$ (5 in the CCEs experiments), 5.3 KCl, 10 HEPES, and 10 glucose, pH 7.3 with NaOH. The intracellular solution contained the following (in mM): 145 glutamic acid, 1 $MgCl_2$, 9 NaCl and 10 HEPES (pH 7.2 adjusted with CsOH). I_{Ca}

were recorded by means of an EPC-10 patch-clamp amplifier (HEKA Elektronik, Lambrecht, Germany) controlled by PULSE software running on a personal computer. The series resistance (*R*s) was monitored until it decreased to < 20 MΩ. *R*s averaged 8.6 ± 0.3 MΩ. The holding potential was -80 mV. I_{Ca} was activated by 50-ms depolarizing voltage steps from -60 to +60 mV in increments of 10-mV between steps. The test voltage protocol was applied every 15 s. Current signals were filtered at 5 kHz and digitized at 50 kHz (online leak was subtracted).

Measurement of cytosolic Ca^{2+} changes $[Ca^{2+}]_c$. BCCs were incubated for 1 h at 37°C in culture medium (DMEM) containing the Ca^{2+} dye fura-2 AM (10 µM). After dye incubation, glass coverslips containing cells were mounted in a chamber. Cells were washed and covered with Tyrode solution composed of the following (in mM): 137 NaCl, 1 $MgCl_2$, 2 $CaCl_2$, 5.3 KCl, 10 HEPES and 10 glucose (pH 7.3 adjusted with NaOH). Microscope fluorescence setup was composed of a Leica DMI 4000 B inverted light microscope (Leica Microsystems, Barcelona, Spain) equipped with an oil immersion objective (Leica x40 Plan Apo; numerical aperture: 1.25) and an intensified charge-coupled device camera (Hamamatsu camera controller C10600 orca R2). During experiments, cells were continuously superfused by means of a five-way superfusion system at 1 ml/min with a common outlet 0.28-mm tube driven by electrically controlled valves with Tyrode solution or Tyrode with drugs dilutions at room temperature. Fura-2 in cells was excited alternatively at 340 ± 10 and 387 ± 10 nm using a Küber CODIX xenon 8 lamp (Leica). Emitted fluorescence was collected through a 540 ± 20 nm emission filter and measured with the camera. Images generated at 1-s intervals were digitally stored and analyzed using LAS AF software (Leica).

SH-SY5Y cell culture and neuroprotection against K^+ and Rotenone/oligomycin A. The human neuroblastoma cell line SH-SY5Y were maintained in a 1:1 mixture of

F-12 Nutrient Mixture (Ham12) (Sigma–Aldrich, Madrid, Spain) and DMEM supplemented with 15 nonessential amino acids, 10 % heat-inactivated FBS, 100 units/ml penicillin, and 100 μg/ml streptomycin (reagents from Invitrogen, Madrid, Spain) in flasks and maintained at 37 °C in a humidified atmosphere of 5 % CO_2 and 95% air. Cells were used in passages 4-13. For the experiments, cells were sub-cultured in 48-well plates at a seeding density of 1×10^4 cells per well. K^+ at 70 mM caused cell depolarization, inducing cytosolic Ca^{2+} overload and consequently, cell death. Rotenone (30 μM) and oligomycin A (10 μM) mixture inhibits complexes I and V of the electron transport chain of the mitochondria, respectively, causing oxidative stress and finally, cell death. At the end of the experiment, cell viability was measured by MTT reduction.

Quantification of viability by MTT in cells (neuroprotection and toxicity experiments) and hippocampal slices. To measure cell viability MTT method was performed as previously described.[52] Briefly, the cell viability was indirectly determined through the ability of the alive cells to reduce the tetrazolium ring of MTT (yellow) through mitochondrial dehydrogenases producing precipitated formazan (blue). At the end of the experiment, cells were incubated with 30 μL MTT solution (5 mg/mL), leading to a final concentration of 0.5 mg/mL. After 2 hours at 37ºC, 300 μL of DMSO were added to solubilize the formazan precipitate. Further, in hippocampal slices protocol, slices were collected immediately after the experiment and incubated with MTT (0.5 mg/ml) in Krebs bicarbonate solution for 45 min at 37ºC. The formazan produced in the hippocampal slices was solubilized by adding 100 μl of dimethyl sulfoxide (DMSO), resulting in a colored compound whose optical density was measured in an ELISA microplate reader at 540 nm. Absorbance values obtained in basal slices were normalized as 100 % viability and all variables included in the same experiment were compared to the normalized value.

Rat hippocampal slices preparation. Three months old Sprague Dawley male rats were decapitated under sodium pentobarbital anesthesia (60 mg/kg, i.p.). Forebrains were rapidly removed and placed into ice-cold Krebs bicarbonate dissection buffer (pH 7.4), containing: $MgSO_4$ 10 mM, KH_2PO_4 1.18 mM, NaCl 120 mM, KCl 2 mM, $NaHCO_3$ 26 mM, glucose 11 mM, $CaCl_2$ 0.5 mM and sucrose 200 mM. Hippocampi were dissected and by the use of a Tissue Chopper McIlwain were cut into transverse slices of 300 micrometers. After that, slices were stabilized during 45 min in a continuously bubbled with 95% O_2/5% CO_2 mixture at 34 ºC.

Veratridine treatment in hippocampal slices. Hippocampal slices corresponding to Veratridine group were incubated during 3.5 h in a 1:1 control solution (NaCl 120 mM, KCl 2 mM, $CaCl_2$ 2 mM, $NaHCO_3$ 26 mM, $MgSO_4$ 1.19 mM, KH_2PO_4 1.18 mM and glucose 11 mM) and DMEM at 30 μM concentration of Veratridine. In the same experiment, different slices were treated in presence of ITH14001 (10 μM), Nimodipine or/and CGP37157 at 30 μM. On the other hand, slices corresponding to basal group were incubated in the same solution without veratridine. At the end of the experiment, cell viability was measured by MTT reduction and 100 % of cell viability was considered the obtained basal group viability.

Glutamate excitotoxicity in rat hippocampal slices. There is a very well-known relationship between glutamate receptor over-activation, Ca^{2+} overload and neuronal cell death occurring during the ischemic cascade. To induce glutamate excitotoxicity, the protocol described by Molz and co-workers was followed.[53] Briefly, after rat hippocampal slices stabilization period, a group of slices were incubated in a nutritive culture medium composed of 50 % of KRB, 50 % of DMEM, 20 mM of HEPES, 100 units/mL penicillin and 100 μg/mL streptomycin containing glutamate (1 mM) at 37 °C in a 95 % O_2/5 % CO_2 atmosphere for 4 h. Different sets of slices were randomly

selected and incubated in the same solution but in presence of 1, 10, 30 μM of ITH14001, 30 μM of nimodipine and 30 μM of CGP37157 for 4 h. Different slices incubated in the mentioned medium without glutamate were considered as basal group and taken as 100 % of cell viability.

Oxygen and glucose deprivation in rat hippocampal slices. Hippocampal slices corresponding to the basal group were incubated during two periods, 15 min and 2 h in a Krebs control solution with the following composition: KCl 2 mM, $NaHCO_3$ 26 mM, $MgSO_4$, NaCl 120 mM, $CaCl_2$ 2 mM, 1.19 mM, KH_2PO_4 1.18 mM and glucose 11 mM; this solution was equilibrated with 95 % O_2/5 % CO_2. A different set of hippocampal slices, corresponding to oxygen and glucose deprivation (OGD) group, were incubated during 15 min in a glucose-free Krebs solution, equilibrated with a 95 % N_2/5 % CO_2 gas mixture; glucose was replaced by 2-deoxyglucose. After the first period, slices were returned back to an oxygenated normal Krebs solution containing glucose (reoxygenation period) for an additional two hour period. In parallel, different slices were treated after OGD period, during de reoxygenation period with 1, 10, 30 μM of ITH14001, 10 μM of nimodipine or/and 10 μM of CGP37157. At the end of the experiment, MTT reduction was measured and cell viability was normalized to basal conditions; basal MTT reduction was considered 100 % of cell viability.

Reactive Oxygen Species (ROS) production measurement in OGD hippocampal slices. After OGD experiment described above, hippocampal brain slices of each group (basal, OGD, and treated with 10 μM of ITH14001) were subjected to the fluorescence probe H_2DCFDA (2',7'-dichlorodihydrofluorescein diacetate) with the aim of measuring ROS production. With this purpose, hippocampal slices were loaded with 10 μM CM-H_2DCFDA and 1 μg/ml Hoechst 33342 (Hoechst) for 30 min at 37°C. CM-H_2DCFDA crosses the cell membrane and is hydrolyzed by intracellular esterases to the non-

fluorescent form, dichlorodihydrofluorescein; later, it reacts with intracellular H_2O_2 (which are highly produced due to OGD experiment) to form dichlorofluorescein, a green fluorescent dye. Using an inverted fluorescence microscope (inverted NIKON eclipse T2000-U microscope), hippocampal CA1 region fluorescence was measured and normalized to Hoechst fluorescence (which stains cell nuclei). Fluorescence analysis was performed using the Metamorph program version 7.0.

Western Blotting Analysis. At the end of the OGD experiment, hippocampal slices were lysed in 100 μL ice-cold lysis buffer (1 % Nonidet P-40, 10 % glycerol, 1 mmol/l phenylmethylsulfonyl fluoride, 1 mmol/l sodium pyrophosphate, 137 mmol/l NaCl, 20 mmol/l Tris-HCl, pH 7.5, 1 μg/ml leupeptin, 20 mmol/l NaF , and 1 mmol/l Na_3VO_4). After protein concentration measurement by the BCA kit (Sigma-Aldrich, Madrid, Spain), protein (30 μg) from the slice lysates was resolved by sodium dodecyl sulfate-polyacrylamide gel electrophoresis. Later, they were transferred to Inmobilon-P membranes (Millipore Iberica SA, Madrid, Spain). Membranes were then incubated with the following antibodies: anti-iNOS (BD Transduction Laboratories, USA) at 1:1000 and anti-β-actin at 1:100,000 (Sigma, Madrid, Spain); Appropriate peroxidase-conjugated secondary antibodies at 1:10,000 were used to detect proteins by enhanced chemiluminescence. Appropriate peroxidase-conjugated secondary antibodies (1:10000) were used and chemoluminiscence was detected by Advance Western-blotting Detection Kit (GE Healthcare, Barcelona, Spain). Finally, optical density was quantified using Scion Image® Alpha 4.0.3.2 program.

Mixed glial cell cultures. Mixed glial cells were obtained from 2-5 days post-natal Sprague Dawley rats. After decapitation, forebrains were obtained; meninges and blood vessels were removed, and mechanically dissociated in DMEM/F12 medium supplemented with 20 % of SBF. Cells were then centrifuged at 1000 rom for 8 min.

The pellets were re-suspended in fresh media and seeded at $40x10^4$ cells/well in 96 well dishes and culture at 37ºC in humidified 5 % CO_2/95 % O_2 chamber. Medium was replaced by DMEM/F12 medium supplemented with 10 % of SBF after 5 days in culture and 7-10 days after experiments were performed.

Anti-inflammatory capacity, measured as nitrite production in primary mixed glial cells culture. After 7 to 10 days in culture, glial cells were pre-incubated with increasing concentrations of the neuroprotective compounds ITH14001 (1, 10 and 30 μM) for 24 h. Then, cells were co-incubated in presence or/and absence of ITH14001, at 1, 10 and 30 μM with LPS (which induces nitrite production) at 1 μg/ml for additional 18 h. Later, nitrite production was measured by modified Griess assay. Briefly, 150 μl of the supernatant were mixed with 75 μl of NEDA and 75 μl of DAPSONE for 5 min at room temperature. Absorbance was measured at 550 nm in an ELISA microplate reader. All data were normalized to basal conditions, considering this value as 100 % of nitrite production.

DPPH reduction assay. Experimental conditions were adapted form previously reported.[54] Briefly, compounds (50 μL) at the desired concentration (0.1 and 1 mM) in ethanol were added to a solution of DPPH in ethanol/water (60/40) (450 μL, 100 μM final concentration**)** and the final solution was kept 15 min in the dark. Thereafter, 200 μL of each variable were placed in a clear bottom black 96-well plate in duplicate. Then, DPPH absorbance of blank (EtOH/water), control (DPPH 100 μM) and compounds plus DPPH were measured at 540 nM in a Fluostar Optima plate-reader (BMG Labtech, Ortenberg, Germany) in triplicate. Results are expressed as % of absorbance reduction of control after subtracting blank absorbance.

AREc32 cells culture. AREc32 cells, generated from MCF-7 breast cancer cells stably expressing luciferase after EpRE sequences, were kindly provided by Prof.

Roland Wolf (University of Dundee, UK).[55] AREc32 cells were cultured in DMEM with glutamax and high glucose, supplemented with 1 % penicillin-streptomycin (10,000 units), geneticin (0.8 mg/ml) and 10 % FBS, at 37ºC in a 5 % CO_2 air atmosphere.

Nrf2 induction by luciferase activity. AREc32 cells constitutively express the plasmid pGL-8xARE that implements 8 copies of the ARE sequences followed by luciferase reporter gene. Cells were sub-cultured in 96-well white plates at the density of $2x10^4$ cells/well. After 24 h, cells were incubated in presence of increasing concentrations (1, 10 and 30 μM) of each compound in duplicate for additional 24 h. Then, following manufacturers protocol Luciferase Assay System (Promega E1500, Madrid, Spain) was performed and luminescence was quantified in an Orion II microplate luminometer (Berthold, Germany). Increase in luciferase activity is due to ARE sequences activation, which is proportional to Nrf2 induction. Fold increase of luciferase activity was normalized to basal conditions.

HepG2 hepatoblastoma cells culture. HepG2 cells were maintained in EMEM supplemented with 10 % FBS, 1 % streptomycin-penicilin (10,000 units), in a 37 ºC humidified atmosphere of 95 % air and 5 % CO_2. HepG2 cells were subcultured in 96-well plates at density of $1x10^5$ cells/well for toxicity studies. For treatments, 1% FBS was used unless stated.

Toxicological evaluation: SH-SY5Y and HepG2 hepatoblastoma cell line. Potential neurotoxicity and hepatotoxicity of ITH14001 compound was measured. For this purpose, both, SH-SY5Y neuroblastoma cell line, and the HepG2 hepatoblastoma cell lines were used. Once cells were sub-cultured and appropriately grown up (70 %), cells were treated in presence of increasing concentrations (1, 3, 10, and 30 μM) of the

compound of interest, ITH14001. After 24 h, cell viability was measured and 100 % of cell viability was considered non-treated cells value.

Statistical analysis. Statistical analyses were performed by GraphPad Prism 5.0 programme. Results were expressed as means ± standard error of the mean. One-way ANOVA followed by Newman-Keuls *pos-hoc* test was used when there were more than two groups. Statistical significance was considered when $p < 0.05$.

ASSOCIATED CONTENT

Supporting information. The supporting information is available free of charge at http://pubs.acs.org

AUTHOR INFORMATION

Corresponding author

*Dr. Rafael León, Mailing address: Instituto Teofilo Hernando y Departamento de Farmacología y Terapéutica, Facultad de Medicina, Universidad Autónoma de Madrid, 28029, Madrid, Spain. Instituto de Investigación Sanitaria, Hospital Universitario de la Princesa, C/ Diego de León, 62, 28006 Madrid, Spain. E-mail: rafael.leon@uam.es Telephone: + 34-91-497-2766. Fax: + 34-91-497-3120.

*Prof. José Carlos Menéndez. Departamento de Química Orgánica y Farmacéutica, Facultad de Farmacia, Universidad Complutense, 28040 Madrid, Spain. Fax: 34-91-3941822; Tel: 34-91-3941840; E-mail: josecm@farm.ucm.es.

Author contributions

I. B. ‡ participated in the pharmacological study design, data acquisition and analysis, drafting and critical revision of the manuscript. G.T.‡ has participated in the design and synthesis of new hybrid ITH14001 and critical revision of the manuscript. P. M.‡ has participated in the design of pharmacological experiments, in the data acquisition and analysis of Nrf2 induction experiments, drafting and critical revision of the manuscript. I. M. and F. P.N. have contributed to data acquisition and data analysis/interpretation of calcium currents inhibition and critical revision of the manuscript. MGL have contributed to pharmacological data analysis/interpretation, and critical revision of the manuscript. M.T.R has contributed to structure design and synthesis supervision, and critical revision of the manuscript. A. G. G. has contributed to concept/design and critical revision of the manuscript and approval of the article. J.C.M. has contributed to concept/design, synthesis supervision, drafting of the manuscript, critical revision of the manuscript and approval of the article. R.L. has contributed to concept/design, drafting of the manuscript, critical revision of the manuscript and approval of the article.. ‡These authors contributed equally.

Funding Sources

RL thank IS Carlos III for research contract under Miguel Servet Program. This work was supported by the following grants to RL: European Commission-ERC, People (Marie Curie Actions) FP7 under REA grant agreement n° PCIG11-GA-2012-322156; Spanish Ministry of Health (Instituto de Salud Carlos III) (grant PI14/00372) and Miguel Servet (CP11/00165); Bayer A.G., “From Targets to Novel Drugs” program (grant 2015-03-1282) and Fundación FIPSE (grant 12-00001344-15) to R.L.; Financial support from MINECO to JCM (grant CTQ2015-68380-R), to AGG (SAF2013-44108-P) and to M.G.L. (SAF2015-63935-R) is also gratefully acknowledged. A.G.G also

thanks BioIberica (CABICYC). P.M. thanks MECD for FPU fellowship (AP2010-1219). G.T. thanks Universidad Complutense for a predoctoral fellowship.

Notes

Authors declare no competing financial interest.

ACKNOWLEDGMENTS

We thank the continued support of Fundación Teófilo Hernando and Fundación de Investigación Biomédica, Hospital Universitario de la Princesa. RL thank IS Carlos III for research contract under Miguel Servet Program.

ABBREVIATION

BCC, bovine chromaffin cells; Ca^{2+}, Calcium ion; $[Ca^{2+}]_c$, Cytosolic calcium concentration; $[Ca^{2+}]_m$, Mitochondrial calcium concentration; $Ca_V1.2$, L-type VDCC subtype; $Ca_V1.3$, L-type VDCC subtype; DPPH, α,α-difenil-ß-picrilhidrazilo radical; ECC, Embryo rats chromaffin cells; GCLc, Glutathione-C-ligase catalytic subunit; HO-1, Heme-oxygenase-1; H_2DCFDA, 2',7'-dichlorodihydrofluorescein diacetate; iNOS, Inducible nitric oxide synthase; I_{Ca}, Calcium current peak; K^+, Potassium ion; LPS, Lipopolysaccharide; mCC, Mitochondrial Ca^{2+} cycling; mNCX, mitochondrial Na^+/Ca^{2+} exchanger; Na^+, Sodium ion; Nrf2, nuclear factor E2-related factor 2; OGD, Oxygen and glucose deprivation; OGD/reox, oxygen and glucose deprivation followed by re-oxygenation; ORAC, oxygen radical arbsorbance capacity; reox, re-oxygenation; RNS, reactive nitrogen species; ROS, reactive oxygen species; rote/olig, rotenone and oligomycin A combination; tPA, tissue plasminogen activator; VDCC, voltage dependent calcium channel.

REFERENCES

(1) Gorlach, A.; Bertram, K.; Hudecova, S.; Krizanova, O., 2015, Calcium and ROS: A mutual interplay. *Redox Biol. 6*, 260-71.

(2) Carraro, M.; Bernardi, P., 2016, Calcium and reactive oxygen species in regulation of the mitochondrial permeability transition and of programmed cell death in yeast. *Cell calcium*.

(3) Toth, A. B.; Shum, A. K.; Prakriya, M., 2016, Regulation of neurogenesis by calcium signaling. *Cell calcium*.

(4) Ureshino, R. P.; Rocha, K. K.; Lopes, G. S.; Bincoletto, C.; Smaili, S. S., 2014, Calcium signaling alterations, oxidative stress, and autophagy in aging. *Antioxid. Redox Signal. 21* (1), 123-37.

(5) Bhosale, G.; Sharpe, J. A.; Sundier, S. Y.; Duchen, M. R., 2015, Calcium signaling as a mediator of cell energy demand and a trigger to cell death. *Ann. N. Y. Acad. Sci. 1350*, 107-16.

(6) Leybaert, L.; Sanderson, M. J., 2012, Intercellular Ca(2+) waves: mechanisms and function. *Physiol. Rev. 92* (3), 1359-92.

(7) Green, K. N., 2009, Calcium in the initiation, progression and as an effector of Alzheimer's disease pathology. *J. Cell. Mol. Med. 13* (9A), 2787-99.

(8) Zamponi, G. W., 2016, Targeting voltage-gated calcium channels in neurological and psychiatric diseases. *Nat. Rev. Drug Discov. 15* (1), 19-34.

(9) Wallace, J., 2014, Calcium dysregulation, and lithium treatment to forestall Alzheimer's disease - a merging of hypotheses. *Cell calcium 55* (3), 175-81.

(10) Kang, S.; Cooper, G.; Dunne, S. F.; Dusel, B.; Luan, C. H.; Surmeier, D. J.; Silverman, R. B., 2012, CaV1.3-selective L-type calcium channel antagonists as potential new therapeutics for Parkinson's disease. *Nat. Commun. 3*, 1146.

(11) (a) Kristian, T.; Siesjo, B. K., 1998, Calcium in ischemic cell death. *Stroke; a journal of cerebral circulation 29* (3), 705-18; (b) Zhang, Y.; Lipton, P., 1999, Cytosolic Ca2+ changes during in vitro ischemia in rat hippocampal slices: major roles for glutamate and Na+-dependent Ca2+ release from mitochondria. *J. Neurosci. 19* (9), 3307-15.

(12) Ha, Y. M.; Kim, M. Y.; Park, M. K.; Lee, Y. S.; Kim, Y. M.; Kim, H. J.; Lee, J. H.; Chang, K. C., 2012, Higenamine reduces HMGB1 during hypoxia-induced brain injury by induction of heme oxygenase-1 through PI3K/Akt/Nrf-2 signal pathways. *Apoptosis 17* (5), 463-74.

(13) Chen, Z.; Mao, X.; Liu, A.; Gao, X.; Chen, X.; Ye, M.; Ye, J.; Liu, P.; Xu, S.; Liu, J.; He, W.; Lian, Q.; Pi, R., 2015, Osthole, a natural coumarin improves cognitive impairments and BBB dysfunction after transient global brain ischemia in C57 BL/6J mice: involvement of Nrf2 pathway. *Neurochem. Res. 40* (1), 186-94.

(14) Hossmann, K. A., 1994, Glutamate-mediated injury in focal cerebral ischemia: the excitotoxin hypothesis revised. *Brain Pathol. 4* (1), 23-36.

(15) Justin, A.; Sathishkumar, M.; Sudheer, A.; Shanthakumari, S.; Ramanathan, M., 2014, Non-hypotensive dose of telmisartan and nimodipine produced synergistic neuroprotective effect in cerebral ischemic model by attenuating brain cytokine levels. *Pharmacol. Biochem. Behav. 122*, 61-73.

(16) Szydlowska, K.; Tymianski, M., 2010, Calcium, ischemia and excitotoxicity. *Cell calcium 47* (2), 122-9.

(17) Lapchak, P. A., 2011, Emerging Therapies: Pleiotropic Multi-target Drugs to Treat Stroke Victims. *Transl. Stroke Res. 2* (2), 129-35.

(18) (a) Nicolau, S. M.; Egea, J.; Lopez, M. G.; Garcia, A. G., 2010, Mitochondrial Na+/Ca2+ exchanger, a new target for neuroprotection in rat hippocampal slices. *Biochem. Biophys. Res. Commun. 400* (1), 140-4; (b) Nicolau, S. M.; de Diego, A. M.; Cortes, L.; Egea, J.; Gonzalez, J. C.; Mosquera, M.; Lopez, M. G.; Hernandez-Guijo, J. M.; Garcia, A. G., 2009, Mitochondrial Na+/Ca2+-exchanger blocker CGP37157 protects against chromaffin cell death elicited by veratridine. *J. Pharmacol. Exp. Ther. 330* (3), 844-54; (c) Ruiz, A.; Alberdi, E.; Matute, C., 2014, CGP37157, an inhibitor of the mitochondrial Na+/Ca2+ exchanger, protects neurons from excitotoxicity by blocking voltage-gated Ca2+ channels. *Cell Death Dis. 5*, e1156; (d) Sisalli, M. J.; Secondo, A.; Esposito, A.; Valsecchi, V.; Savoia, C.; Di Renzo, G. F.; Annunziato, L.; Scorziello, A., 2014, Endoplasmic reticulum refilling and mitochondrial calcium extrusion promoted in neurons by NCX1 and NCX3 in ischemic preconditioning are determinant for neuroprotection. *Cell Death Differ. 21* (7), 1142-9.

(19) Zhang, Y.; Lipton, P., 1999, Cytosolic Ca2+ changes during in vitro ischemia in rat hippocampal slices: major roles for glutamate and Na+-dependent Ca2+ release from mitochondria. *J Neurosci 19* (9), 3307-15.

(20) Cox, D. A.; Conforti, L.; Sperelakis, N.; Matlib, M. A., 1993, Selectivity of inhibition of Na(+)-Ca2+ exchange of heart mitochondria by benzothiazepine CGP-37157. *J. Cardiovasc. Pharmacol. 21* (4), 595-9.

(21) Pilitsis, J. G.; Diaz, F. G.; O'Regan, M. H.; Phillis, J. W., 2002, Inhibition of mitochondrial Na(+)/Ca(2+) exchange by 7-chloro-5-(2-chlorophenyl)-1,5-dihydro-4,1-benzothiazepin-2(3H)-one attenuates free fatty acid efflux in rat cerebral cortex during ischemia-reperfusion injury. *Neurosci. Lett. 321* (1-2), 1-4.

(22) Li, X. M.; Yang, J. M.; Hu, D. H.; Hou, F. Q.; Zhao, M.; Zhu, X. H.; Wang, Y.; Li, J. G.; Hu, P.; Chen, L.; Qin, L. N.; Gao, T. M., 2007, Contribution of downregulation of L-type calcium currents to delayed neuronal death in rat hippocampus after global cerebral ischemia and reperfusion. *J. Neurosci. 27* (19), 5249-59.

(23) Babu, C. S.; Ramanathan, M., 2011, Post-ischemic administration of nimodipine following focal cerebral ischemic-reperfusion injury in rats alleviated excitotoxicity, neurobehavioural alterations and partially the bioenergetics. *Int. J. Dev. Neurosci. 29* (1), 93-105.

(24) Rosenbaum, D.; Zabramski, J.; Frey, J.; Yatsu, F.; Marler, J.; Spetzler, R.; Grotta, J., 1991, Early treatment of ischemic stroke with a calcium antagonist. *Stroke; a journal of cerebral circulation 22* (4), 437-41.

(25) Labiche, L. A.; Grotta, J. C., 2004, Clinical trials for cytoprotection in stroke. *NeuroRx : the journal of the American Society for Experimental NeuroTherapeutics 1* (1), 46-70.

(26) Tenti, G.; Parada, E.; Leon, R.; Egea, J.; Martinez-Revelles, S.; Briones, A. M.; Sridharan, V.; Lopez, M. G.; Ramos, M. T.; Menendez, J. C., 2014, New 5-unsubstituted dihydropyridines with improved CaV1.3 selectivity as potential neuroprotective agents against ischemic injury. *J. Med. Chem. 57* (10), 4313-23.

(27) (a) Chan, C. S.; Guzman, J. N.; Ilijic, E.; Mercer, J. N.; Rick, C.; Tkatch, T.; Meredith, G. E.; Surmeier, D. J., 2007, Rejuvenation' protects neurons in mouse models of Parkinson's disease. *Nature 447* (7148), 1081-1086; (b) Hurley, M. J.; Brandon, B.; Gentleman, S. M.; Dexter, D. T., 2013, Parkinson's disease is associated with altered expression of CaV1 channels and calcium-binding proteins. *Brain : a journal of neurology 136* (Pt 7), 2077-2097.

(28) Buendia, I.; Michalska, P.; Navarro, E.; Gameiro, I.; Egea, J.; Leon, R., 2016, Nrf2-ARE pathway: An emerging target against oxidative stress and neuroinflammation in neurodegenerative diseases. *Pharmacol. Ther. 157*, 84-104.
(29) (a) Cui, L. Y.; Zhu, Y. C.; Gao, S.; Wang, J. M.; Peng, B.; Ni, J.; Zhou, L. X.; He, J.; Ma, X. Q., 2013, Ninety-day administration of dl-3-n-butylphthalide for acute ischemic stroke: a randomized, double-blind trial. *Chin. Med. J. (Engl) 126* (18), 3405-10; (b) Jia, J.; Wei, C.; Liang, J.; Zhou, A.; Zuo, X.; Song, H.; Wu, L.; Chen, X.; Chen, S.; Zhang, J.; Wu, J.; Wang, K.; Chu, L.; Peng, D.; Lv, P.; Guo, H.; Niu, X.; Chen, Y.; Dong, W.; Han, X.; Fang, B.; Peng, M.; Li, D.; Jia, Q.; Huang, L., 2015, The effects of DL-3-n-butylphthalide in patients with vascular cognitive impairment no dementia caused by subcortical ischemic small vessel disease: A multicentre, randomized, double-blind, placebo-controlled trial. *Alzheimers Dement.*
(30) Fernandez-Morales, J. C.; Arranz-Tagarro, J. A.; Calvo-Gallardo, E.; Maroto, M.; Padin, J. F.; Garcia, A. G., 2012, Stabilizers of neuronal and mitochondrial calcium cycling as a strategy for developing a medicine for Alzheimer's disease. *ACS Chem. Neurosci. 3* (11), 873-83.
(31) Pei, Y.; Lilly, M. J.; Owen, D. J.; D'Souza, L. J.; Tang, X. Q.; Yu, J.; Nazarbaghi, R.; Hunter, A.; Anderson, C. M.; Glasco, S.; Ede, N. J.; James, I. W.; Maitra, U.; Chandrasekaran, S.; Moos, W. H.; Ghosh, S. S., 2003, Efficient syntheses of benzothiazepines as antagonists for the mitochondrial sodium-calcium exchanger: potential therapeutics for type II diabetes. *J. Org. Chem. 68* (1), 92-103.
(32) Chavan, S. P.; Subbarao, Y. T.; Dantale, S. W.; Sivappa, R., 2001, Transesterification of ketoesters using AMBERLYST-15. *Synth. Commun. 31*, 289-294.
(33) Poindexter, G. S.; Temple, D. L. 1985.
(34) (a) Garcia-Palomero, E.; Renart, J.; Andres-Mateos, E.; Solis-Garrido, L. M.; Matute, C.; Herrero, C. J.; Garcia, A. G.; Montiel, C., 2001, Differential expression of calcium channel subtypes in the bovine adrenal medulla. *Neuroendocrinology 74* (4), 251-61; (b) Garcia, A. G.; Garcia-De-Diego, A. M.; Gandia, L.; Borges, R.; Garcia-Sancho, J., 2006, Calcium signaling and exocytosis in adrenal chromaffin cells. *Physiol. Rev. 86* (4), 1093-131.
(35) Caricati-Neto, A.; Padin, J. F.; Silva-Junior, E. D.; Fernandez-Morales, J. C.; de Diego, A. M.; Jurkiewicz, A.; Garcia, A. G., 2013, Novel features on the regulation by mitochondria of calcium and secretion transients in chromaffin cells challenged with acetylcholine at 37 degrees C. *Physiol. Rep. 1* (7), e00182.
(36) Fernandez-Morales, J. C.; Padin, J. F.; Arranz-Tagarro, J. A.; Vestring, S.; Garcia, A. G.; de Diego, A. M., 2014, Hypoxia-elicited catecholamine release is controlled by L-type as well as N/PQ types of calcium channels in rat embryo chromaffin cells. *Am. J. Physiol. Cell Physiol. 307* (5), C455-65.
(37) Maroto, R.; De la Fuente, M. T.; Artalejo, A. R.; Abad, F.; Lopez, M. G.; Garcia-Sancho, J.; Garcia, A. G., 1994, Effects of Ca2+ channel antagonists on chromaffin cell death and cytosolic Ca2+ oscillations induced by veratridine. *European journal of pharmacology 270* (4), 331-339.
(38) Ashton, D.; Willems, R.; Marrannes, R.; Janssen, P. A., 1990, Extracellular ions during veratridine-induced neurotoxicity in hippocampal slices: neuroprotective effects of flunarizine and tetrodotoxin. *Brain Res. 528* (2), 212-22.
(39) Galkin, A.; Abramov, A. Y.; Frakich, N.; Duchen, M. R.; Moncada, S., 2009, Lack of oxygen deactivates mitochondrial complex I: implications for ischemic injury? *J. Biol. Chem. 284* (52), 36055-61.

(40) Gonzalez-Lafuente, L.; Egea, J.; Leon, R.; Martinez-Sanz, F. J.; Monjas, L.; Perez, C.; Merino, C.; Garcia-De Diego, A. M.; Rodriguez-Franco, M. I.; Garcia, A. G.; Villarroya, M.; Lopez, M. G.; de Los Rios, C., 2012, Benzothiazepine CGP37157 and its isosteric 2'-methyl analogue provide neuroprotection and block cell calcium entry. *ACS Chem. Neurosci. 3* (7), 519-29.
(41) Choi, D. W., 1988, Glutamate neurotoxicity and diseases of the nervous system. *Neuron 1* (8), 623-34.
(42) Abramov, A. Y.; Duchen, M. R., 2010, Impaired mitochondrial bioenergetics determines glutamate-induced delayed calcium deregulation in neurons. *Biochim. Biophys. Acta 1800* (3), 297-304.
(43) Molz, S.; Dal-Cim, T.; Budni, J.; Martin-de-Saavedra, M. D.; Egea, J.; Romero, A.; del Barrio, L.; Rodrigues, A. L.; Lopez, M. G.; Tasca, C. I., 2011, Neuroprotective effect of guanosine against glutamate-induced cell death in rat hippocampal slices is mediated by the phosphatidylinositol-3 kinase/Akt/ glycogen synthase kinase 3beta pathway activation and inducible nitric oxide synthase inhibition. *Journal of neuroscience research 89* (9), 1400-8.
(44) Chen, H.; Yoshioka, H.; Kim, G. S.; Jung, J. E.; Okami, N.; Sakata, H.; Maier, C. M.; Narasimhan, P.; Goeders, C. E.; Chan, P. H., 2011, Oxidative stress in ischemic brain damage: mechanisms of cell death and potential molecular targets for neuroprotection. *Antioxid. Redox. Signal. 14* (8), 1505-1517.
(45) Lakhan, S. E.; Kirchgessner, A.; Hofer, M., 2009, Inflammatory mechanisms in ischemic stroke: therapeutic approaches. *J. Transl. Med. 7*, 97.
(46) Chamorro, A.; Dirnagl, U.; Urra, X.; Planas, A. M., 2016, Neuroprotection in acute stroke: targeting excitotoxicity, oxidative and nitrosative stress, and inflammation. *Lancet Neurol. 15* (8), 869-81.
(47) Gao, Y.; Chu, S. F.; Li, J. P.; Zhang, Z.; Yan, J. Q.; Wen, Z. L.; Xia, C. Y.; Mou, Z.; Wang, Z. Z.; He, W. B.; Guo, X. F.; Wei, G. N.; Chen, N. H., 2015, Protopanaxtriol protects against 3-nitropropionic acid-induced oxidative stress in a rat model of Huntington's disease. *Acta Pharmacol. Sin. 36* (3), 311-22.
(48) (a) Fu, Y.; Liu, Q.; Anrather, J.; Shi, F. D., 2015, Immune interventions in stroke. *Nat. Rev. Neurol. 11* (9), 524-35; (b) Smith, C. J.; Denes, A.; Tyrrell, P. J.; Di Napoli, M., 2015, Phase II anti-inflammatory and immune-modulating drugs for acute ischaemic stroke. *Expert Opin. Investig. Drugs 24* (5), 623-43.
(49) Moro, M. A.; Lopez, M. G.; Gandia, L.; Michelena, P.; Garcia, A. G., 1990, Separation and culture of living adrenaline- and noradrenaline-containing cells from bovine adrenal medullae. *Anal. Biochem. 185* (2), 243-8.
(50) Sorensen, J. B.; Nagy, G.; Varoqueaux, F.; Nehring, R. B.; Brose, N.; Wilson, M. C.; Neher, E., 2003, Differential control of the releasable vesicle pools by SNAP-25 splice variants and SNAP-23. *Cell 114* (1), 75-86.
(51) Rae, J.; Cooper, K.; Gates, P.; Watsky, M., 1991, Low access resistance perforated patch recordings using amphotericin B. *J. Neurosci. Methods 37* (1), 15-26.
(52) Denizot, F.; Lang, R., 1986, Rapid colorimetric assay for cell growth and survival. Modifications to the tetrazolium dye procedure giving improved sensitivity and reliability. *J. Immunol. Methods 89* (2), 271-7.
(53) Molz, S.; Decker, H.; Dal-Cim, T.; Cremonez, C.; Cordova, F. M.; Leal, R. B.; Tasca, C. I., 2008, Glutamate-induced toxicity in hippocampal slices involves apoptotic features and p38 MAPK signaling. *Neurochem. Res. 33* (1), 27-36.
(54) Dudonne, S.; Vitrac, X.; Coutiere, P.; Woillez, M.; Merillon, J. M., 2009, Comparative study of antioxidant properties and total phenolic content of 30 plant

extracts of industrial interest using DPPH, ABTS, FRAP, SOD, and ORAC assays. *J. Agric. Food. Chem. 57* (5), 1768-74.

(55) Wang, X. J.; Hayes, J. D.; Wolf, C. R., 2006, Generation of a stable antioxidant response element-driven reporter gene cell line and its use to show redox-dependent activation of nrf2 by cancer chemotherapeutic agents. *Cancer Res. 66* (22), 10983-94.

Table of contents

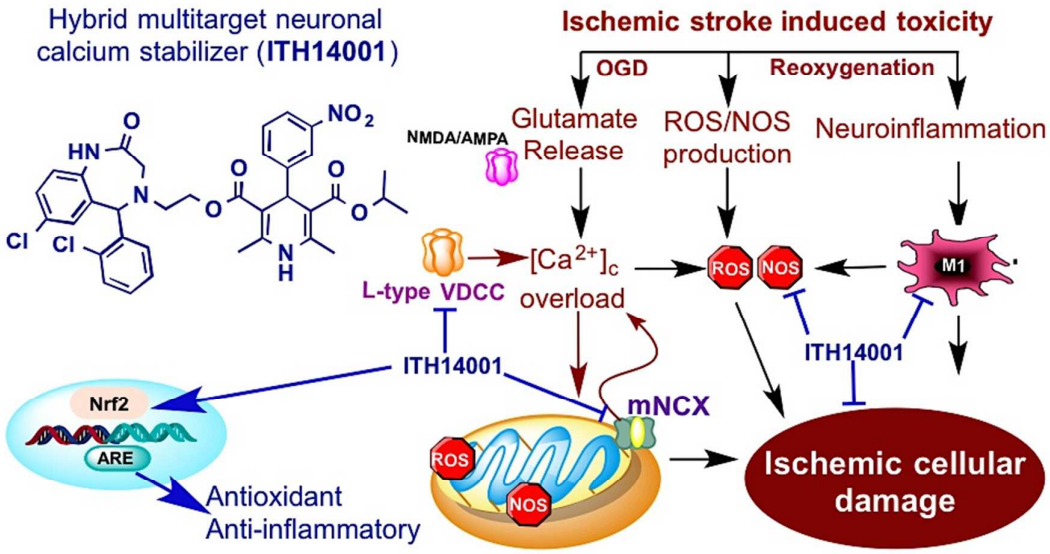
Hybrid multitarget neuronal calcium stabilizer (ITH14001)
Ischemic stroke induced toxicity
OGD
Reoxygenation
Glutamate Release
ROS/NOS production
Neuroinflammation
NMDA/AMPA
L-type VDCC
[Ca2+]c overload
ROS
NOS
M1
ITH14001
ITH14001
mNCX
Nrf2
ARE
Antioxidant
Anti-inflammatory
Ischemic cellular damage

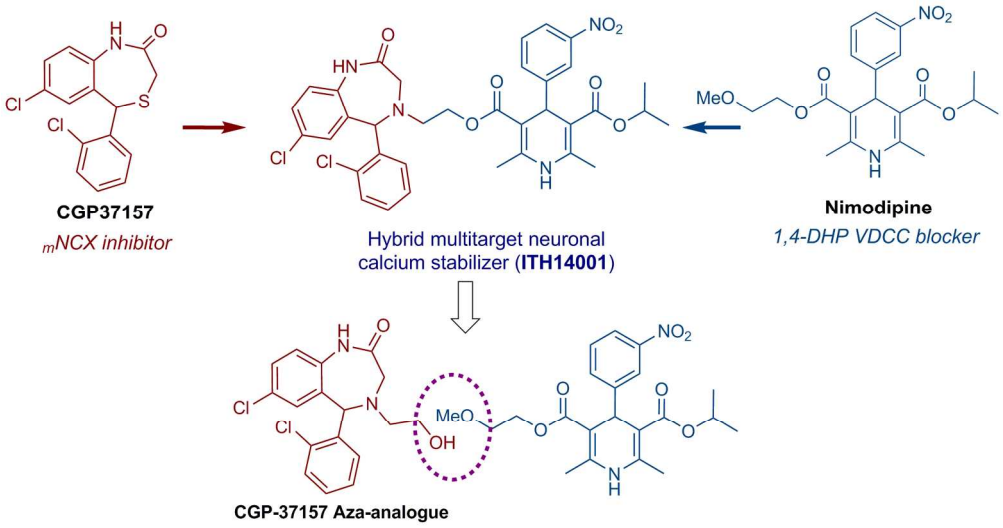

Figure 1. Rational design of the multitarget neuronal calcium stabilizer ITH14001.

178x94mm (300 x 300 DPI)

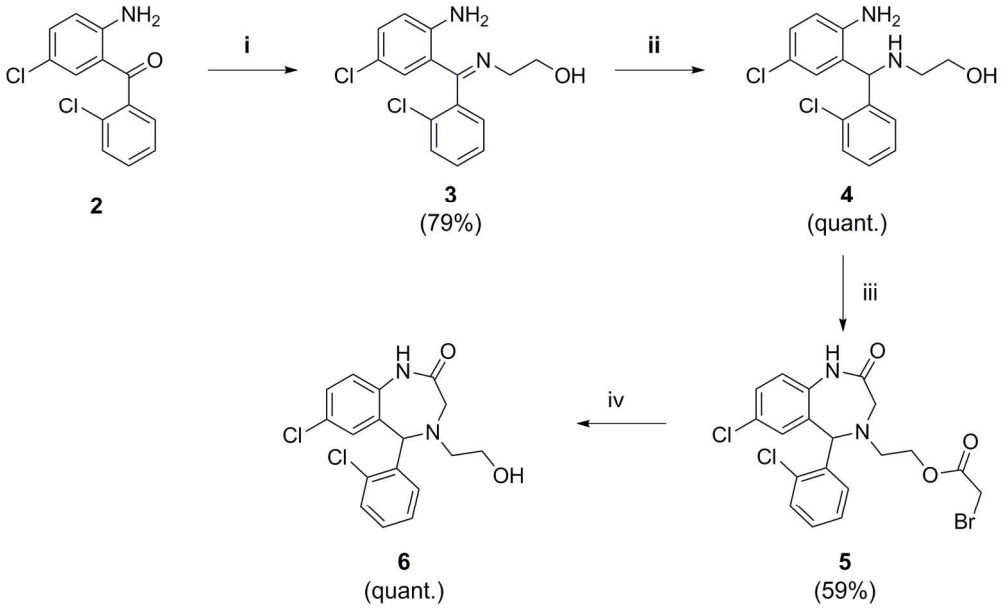

Scheme 1. Synthesis of the aza-analogue of CGP37157 6. Reagents and conditions: (i) 2-aminoethanol (neat), 140 ºC, 20 h; (ii) NaBH3(CN), MeOH/AcOH, 0 ºC to room temperature, 18 h; (iii) (a) bromoacetyl bromide, 0 ºC to room temperature, 17 h; (b) DIEA, 50 ºC, 5 h; (iv) 2 M aqueous KOH, MeOH, room temperature, 2 h.

166x101mm (300 x 300 DPI)

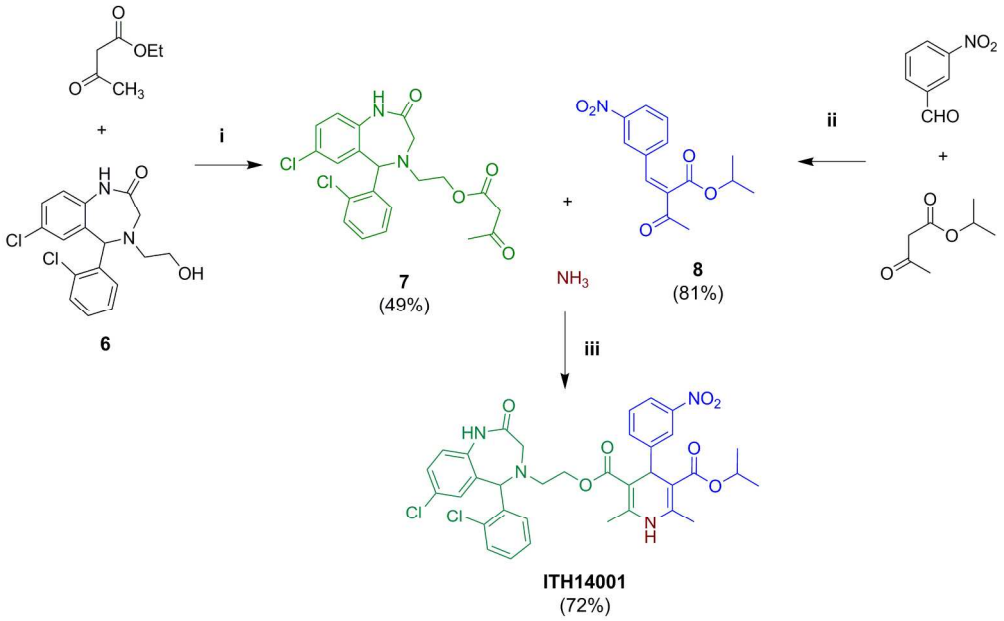

Scheme 2. Multicomponent synthesis of the hybrid compound ITH14001. Reagents and conditions: (i) Amberlist-15, toluene, reflux, 15 h; (ii) Piperidine, AcOH, benzene, reflux, 16 h; (iii) EtOH, reflux, 15 h.

202x125mm (300 x 300 DPI)

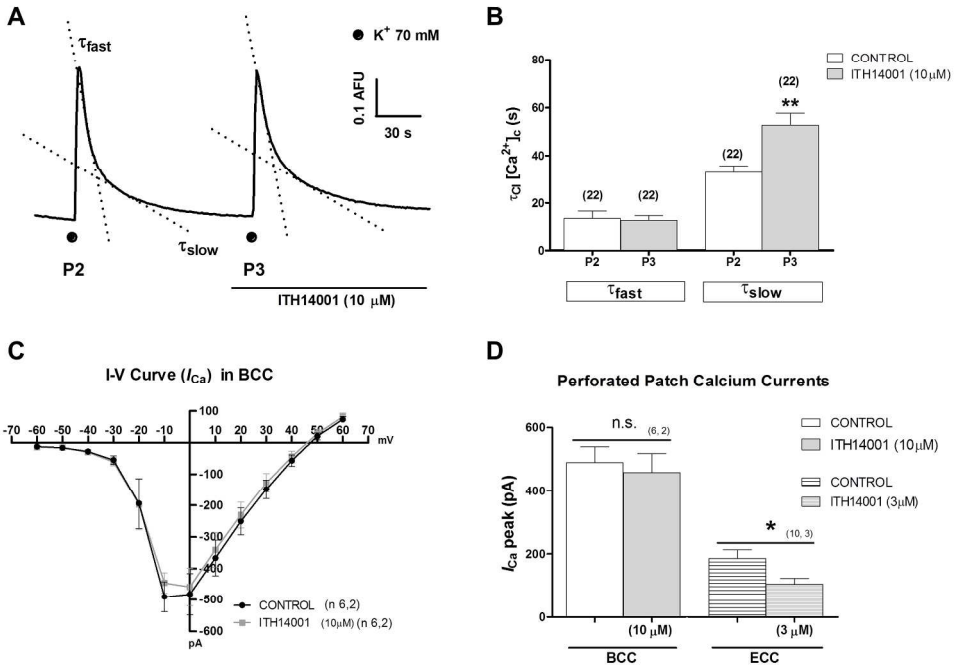

Figure 2. A) Representative traces of [Ca2+]c evoked by K+ pulses (5 s, 70 mM) in BCCs. [Ca2+]c measurements were done with Fura-2 AM dye (1 h incubation, 10 μM). P2 and P3 represent the second and the third pulse under compound (ITH14001, 10 μM) incubation. B) Quantification of both (fast and slow) clearance time constant of the [Ca2+]c peaks represented in A. C) Intensity-voltage (I-V) calcium current curve elicited by 50-ms depolarizing pulses in BCCs under the perforated patch configuration. I-V curves were performed perfusing the cells with tyrode medium (Control) or tyrode with ITH14001 (10 μM). D) Quantification of the calcium current peak (ICa) in BCCs or in embryo chromaffin cells (ECCs) without (control) or with ITH14001 treatment in BCCs (3 μM) and in ECCs (10 μM). Data are mean ± SEM of triplicates of four independent experiments: *p < 0.05 compared with control; **p < 0.01, compared with control conditions.

254x190mm (300 x 300 DPI)

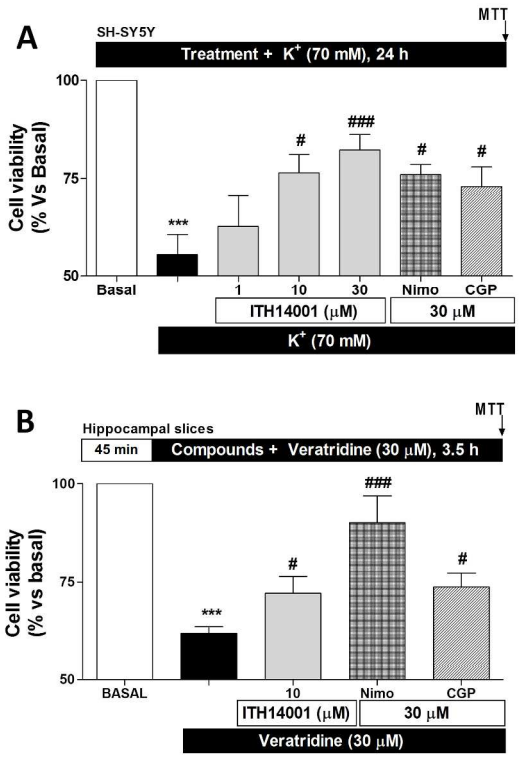

Figure 3. Neuroprotective effect of ITH14001 against [Ca2+]c overload: A) neuroprotective effect of ITH14001 against the cytotoxic effect induced by high K+ (70 mM). Cells were co-incubated with increasing concentrations of ITH14001 or control compounds (nimodipine and CGP37157, 30 μM) and high K+ during 24 h. B) Cytoprotective effect against the toxicity elicited in rat hippocampal slices by veratridine (30 μM) during 3.5 h alone or co-incubated with the indicated treatments. Data are expressed as mean ± SEM of four different experiments in triplicate. ***p < 0.001 compared with basal conditions; ###p < 0.001 and #p < 0.05 compared with the corresponding toxic stimulus.

762x575mm (96 x 96 DPI)

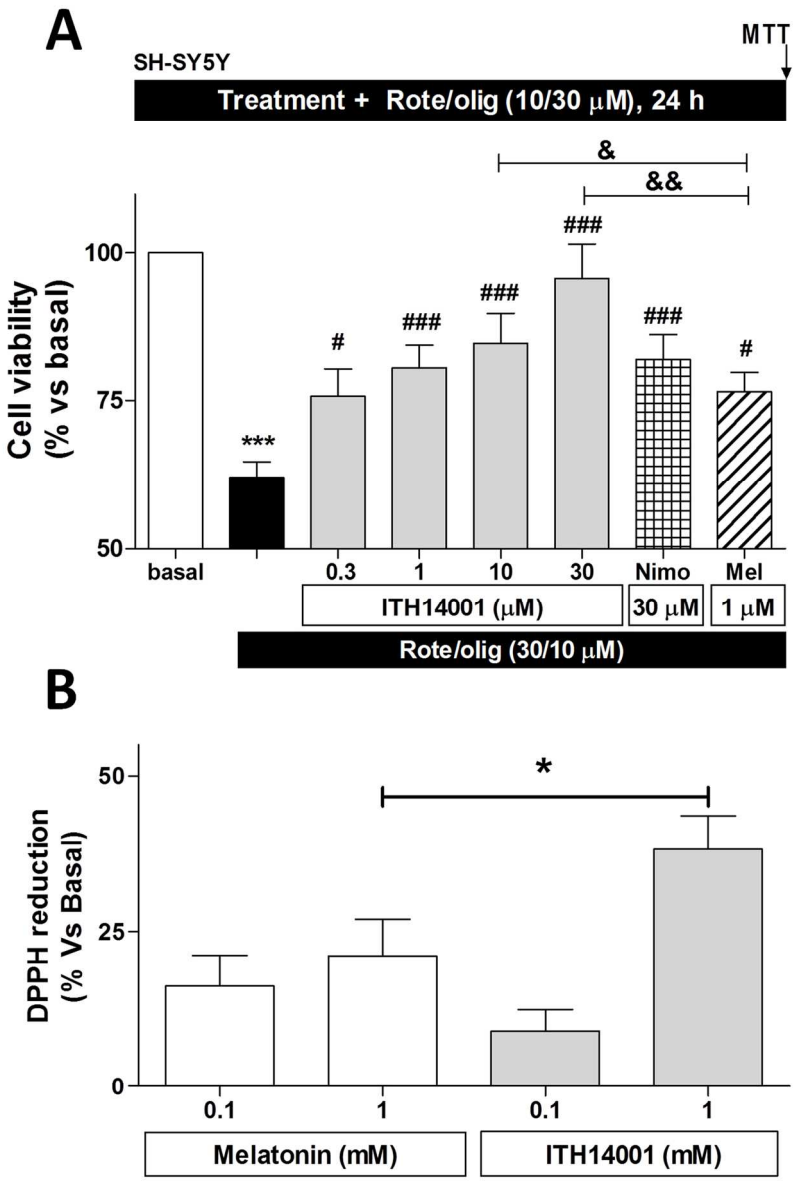

Figure 4. Neuroprotective effect against oxidative stress and DPPH reduction effect of ITH14001: A) protective effect of increasing concentrations of ITH14001 against the toxicity induced by rotenone/oligomycin A (30/10 μM) with a co-incubation protocol during 24 h. Data are expressed as means ± SEM of five different experiments in triplicate. ***p < 0.001 compared to basal conditions; ###p < 0.001 and #p < 0.05 compared to toxic stimulus. &&p < 0.01 and &p < 0.05 compared to melatonin. . B) Scavenger effect of ITH14001 in the DPPH assay compared to the antioxidant neurohormone melatonin. Values are expressed as percentage of DPPH radical reduction as mean ± SEM of four different experiments in triplicate. *p < 0.05 compared with melatonin 1 mM.

132x192mm (300 x 300 DPI)

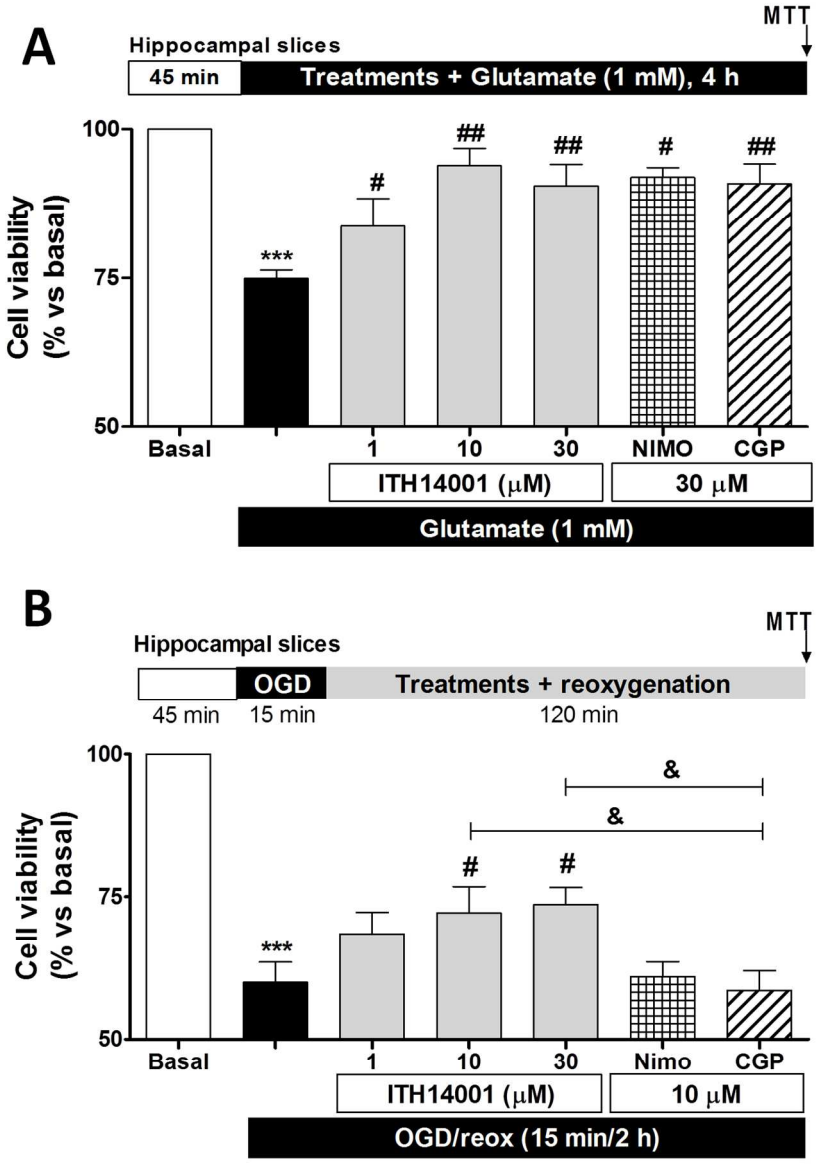

Figure 5. ITH14001 protected rat hippocampal slices against the excitotoxicity elicited by glutamate and the toxicity induced by OGD/reox. A) After the stabilization period (45 min), slices were incubated with glutamate (1 mM) alone or co-incubated with the compounds during 4 h. Thereafter, viability was determined by the MTT method. B) After 45 min stabilization slices were subjected to OGD (15 min) followed by reoxygenation (2 h). Treatments were incubated after the OGD period, during the reoxygenation phase. Thereafter, viability was determined by the MTT method. Data are expressed as mean ± SEM of five different experiments in triplicate. ***$p < 0.001$ compared with basal conditions; ##$p < 0.01$ and #$p < 0.05$ compared with the correspondent toxic stimulus. &$p < 0.05$ compared with CGP37157.

140x192mm (300 x 300 DPI)

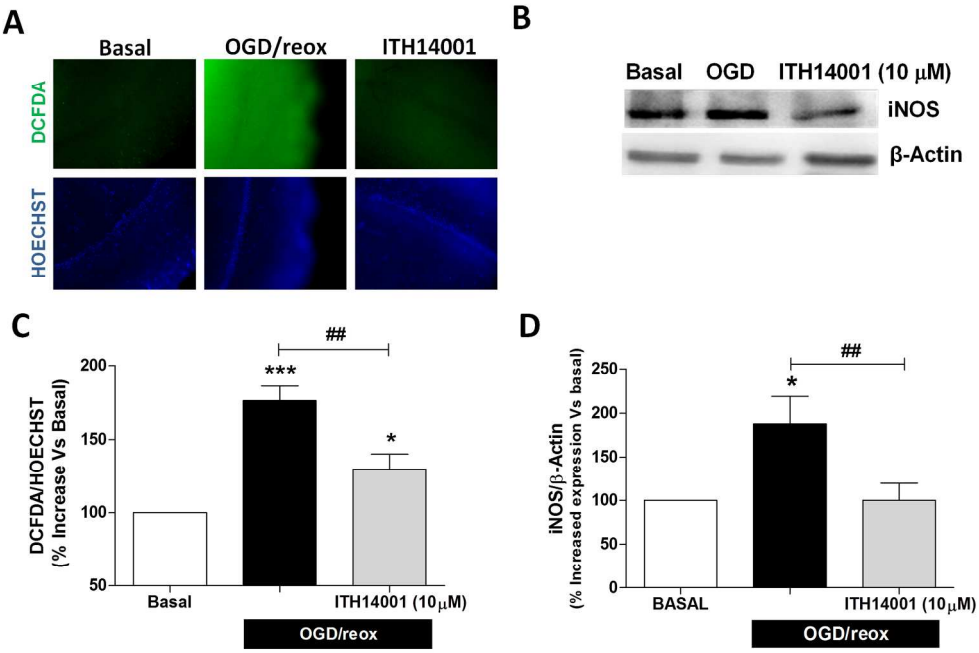

Figure 6. ITH14001 reduces ROS production and iNOS expression in rat hippocampal slices after OGD/reox. ROS production measured as H2DCFDA fluorescence intensity increase after OGD-reox period. Slices were subjected to the same OGD/reox protocol loaded with the fluorescent dye during the stabilization period. Compound ITH14001 was incubated at 10 μM after the 15 min OGD period, during the reox phase. A) Representative microphotographs of ROS production and C) ROS production quantification. Western-blot analysis of iNOS expression in hippocampal slices subjected to OGD/reox alone or incubated post-OGD with ITH14001 (10 μM). B) Representative western blot traces and D) iNOS expression quantification. Data are expressed as mean ± SEM of five different experiments in quadruplicate. ***$p < 0.001$ compared with basal conditions; ##$p < 0.005$ and #$p < 0.05$ compared with the corresponding toxic stimulus.

231x155mm (300 x 300 DPI)

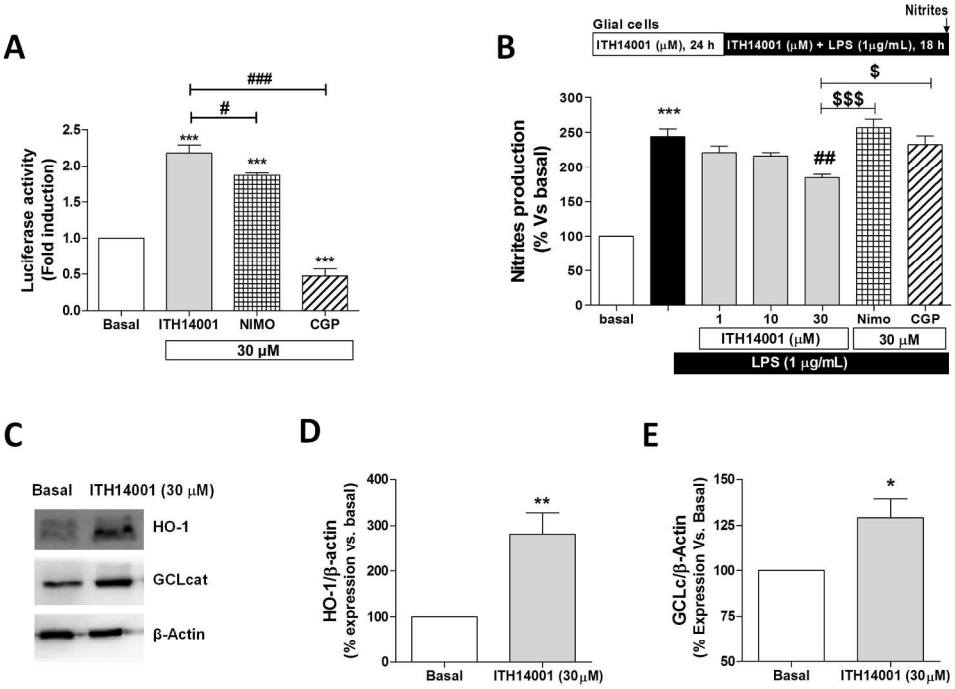

Figure 7. ITH14001 induces the expression of Nrf2-ARE pathway dependent enzymes in AREc32 and glial cells. A) Nrf2 induction in AREc32 cells by ITH14001, nimodipine and CGP37157 at 30 µM. Luciferase relative activity was normalized to control conditions assigning the value of 1. Data are expressed as mean ± SEM of duplicates of five different experiments. ***p < 0.001 compared to basal conditions; ###p < 0.001 and #p < 0.05 compared to ITH14001. B) Reduction of nitrite production by compound ITH14001 upon stimulation of primary glial cultures with LPS (1 µg/mL). Data were normalized to basal conditions (100 %). Data are expressed as mean ± SEM of five different experiments in triplicate. **p < 0.005 compared with basal conditions; #p < 0.05 compared with LPS-induced nitrite production. C) Western-blot analysis of HO-1 and GCLc enzymes induced by ITH14001 (30 µM) in glial cells primary cultures. D) Quantification of HO-1 and E) GCLc over-expression normalized to basal conditions induced by ITH14001 (30 µM). Data are expressed as mean ± SEM of four different cultures. **p < 0.01 and *p < 0.05 compared with basal conditions.

254x192mm (300 x 300 DPI)

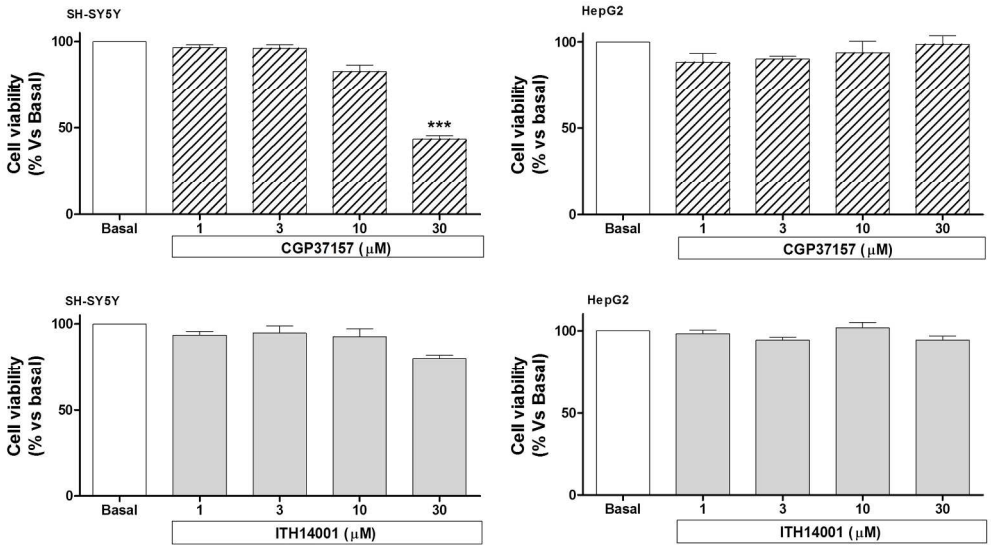

Figure 8: Cytotoxicity elicited by compound ITH14001 and CGP37157 in the neuroblastoma cell line SH-SY5Y and hepatotoxicity in the hepatocarcinoma HepG2 cells. Viability was measured as MTT reduction in presence of increasing concentrations of compounds. Data are expressed as mean ± SEM of four different experiments in triplicate. ***$p < 0.001$ compared to basal conditions.

237x132mm (300 x 300 DPI)

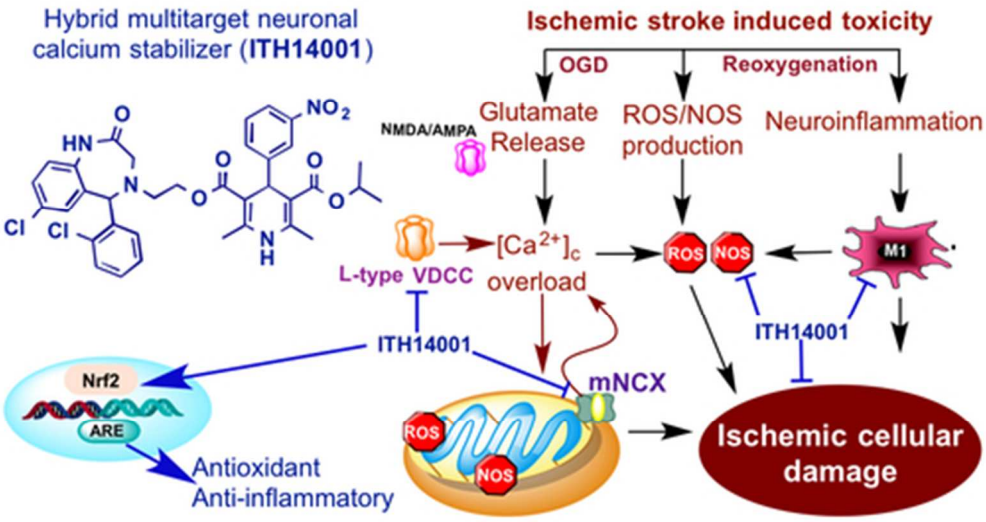

TOC

43x22mm (300 x 300 DPI)